SLAC–PUB–5795
SSCL–538
July 1992
(E/I)

Further Comments about B-Physics in pp Interactions*

M. Botlo, D. Coupal, J. Dorenbosch, A. Fridman◇
J. Siegrist and E. Wang
Superconducting Super Collider
Dallas, Texas 75237

S. Shapiro and J. Va'vra
Stanford Linear Accelerator Center
Stanford University, Stanford, California 94309

N. Johnson and J. Izen
Physics Department, University of Texas-Dallas
Richardson, Texas 75083-0688

R. Lander and S. Mani
Physics Department, University of California at Davis
Davis, California 95616

P. Gutierrez
Department of Physics and Astronomy, University of Oklahoma
Norman, Oklahoma 73071

Abstract

We summarize discussions concerning the study of B-physics at the SSC. Different approaches are considered. The first one corresponds to the collider experiments detecting charged particles with pseudorapidity of $|\eta| \leq 2.4$, whereas the second method considers the detection of B mesons in the forward/backward directions ($|\eta| > 2.4$). The utilization of external or gas-jet targets are also briefly discussed.

---

* Work supported in part by Department of Energy contract DE–AC03–76SF00515.
◇ LPNHE, Université de Paris VI et VII.

Table of Contents

1 - Introduction

In the following we will summarize discussions at the SSCL concerning B-physics that could be investigated in pp interactions. Some of the SSC accelerator properties which may be useful for this type of physics are described in Appendix A. Table 1 presents the cross sections and the production rates expected at the SSC center-of-mass energy ($\sqrt{s} = 40$ TeV). We also compare these values with those that could be obtained with an e^+e^- B-factory. The large number of $B\bar{B}$ events in pp interactions will allow the search for CP violation in B decay. For this discussion we will consider the $B_d^0, \bar{B}_d^0 \to J/\psi K_s^0$ decay.

Table 1 - The comparison of luminosity (L), charged multiplicity ($\langle n \rangle$), total (σ_T) and $b\bar{b}$ ($\sigma(b\bar{b})$) cross sections.[1] The number of interactions with $b\bar{b}$ per year ($N(b\bar{b})/10^7$ s) as well as the number of interactions per second ($N_{\rm int}$/s) are also given.

	SSC (40 TeV)	$e^+e^- \to \Upsilon(4S)$ (0.01 TeV)
L cm^{-2} s^{-1}	10^{32}	3×10^{33}
$\langle n \rangle$	~ 115	~ 12
σ_T	~ 120 mb	4 nb
$\sigma(b\bar{b})$	~ 500 μb	1.2 nb
$\sigma(b\bar{b})/\sigma_T$	$\sim 1/240$	$\sim 1/4$
$N(b\bar{b})/10^7$ s	5×10^{11}	3.6×10^7
$N_{\rm int}$/s	1.2×10^7	1.4×10^1

Let us remember that when searching for CP violation effects, one usually considers a luminosity of $L \simeq 10^{32}$ cm^{-2} s^{-1} in order to decrease the multiple pp interaction per bunch crossing (in principle, the SSC could easily reach $L \geq 10^{33}$ cm^{-2} s^{-1}). For minimum bias events this would correspond to an average of $\langle m \rangle \simeq 0.17$ pp interactions per bunch crossing, and to

$$\frac{P(2)}{P(1)} \simeq 0.08 \ , \qquad \frac{P(3)}{P(1)} \simeq 0.005 \ .$$

Here $P(m)$ is the probability of having m interactions per bunch crossing and is assumed to follow a Poisson distribution. The above values are obtained with an inelastic cross section of $\sigma_T \simeq 100$ mb (Ref. 1). By triggering on a specific signature, however, the fraction of events with multiple interactions is ~ 0.17.

In Section 2 we briefly discuss some aspects of the search for CP violation in B decay. We also examine the possibility that B and $\bar{B}$ may not be produced in equal amounts in pp interactions. We then describe the use of the SSC center-of-mass energy (40 TeV). For these discussions we consider two different approaches. The first one, where the charged B decay particles are emitted with large emission angles $\Theta > 10°$ ($0 \leq \Theta \leq 90°$), corresponding to the pseudorapidity range of $|\eta| \leq 2.4$ and similar to the usual collider experiment projects (Section 3). The second method, where the Bs are emitted in the forward-backward direction with respect to the beam line, will be considered in Section 4. These kinds of experiments are discussed in order to compare their advantages with those obtained in the interactions with p-beams and fixed targets. Note that in this latter case, the $b\bar{b}X$ cross section (X meaning anything) at $\sqrt{s} = 0.19$ TeV is much smaller than that expected at the SSC collider (see below). Comments on using external or gas-jet targets are made in Section 5.

For the discussion of CP violation measurements, we essentially consider the $B_d^0, \bar{B}_d^0 \to J/\psi K_s^0$ decay. Large statistics concerning this decay channel will probably exist at the time the SSC begins operation. This decay has, however, often been studied in order to compare the e^+e^- B-Factory with pp collisions; therefore, the utilization of this decay channel can also be useful in the comparison of the various pp experiments and for comparison with e^+e^- interactions.

2 - Remarks about CP violation measurements

2.1 - General comments

We would like to discuss some aspects of the search for CP violation in B_d^0 ($\bar{B}_d^0$) decays into self-conjugate states f ($f = \bar{f}$). The CP violation causes differences between the decay of $B_d^0 \to f$ and $\bar{B}_d^0 \to f$. For these decays CP violation effects are expected to be larger than in other cases[2,3] ($f \neq \bar{f}$). Moreover, the measured quantities are independent of (unknown) final state interactions.

The mixing phenomena (as well as $f = \bar{f}$) require the tagging of the associated beauty hadrons. In the present discussion, we consider that the tagging is given by the charge of the lepton ($l^{\pm}$) in the semileptonic decay of the associated beauty hadron, $B, \bar{\Lambda}_b \to l^+X$ or $\bar{B}, \Lambda_b \to l^-X$. Here $\Lambda_b \equiv bqq$ ($\bar{\Lambda}_b \equiv \bar{b}\bar{q}\bar{q}$) represents a beauty baryon. One of the usual methods of searching for CP violation consists of comparing the number of l^+fX (N_+) and l^-fX (N_-) events.

The CP violation effect would then be observed if the asymmetry parameter

$$A = \frac{N_+ - N_-}{N_+ + N_-} \neq 0 \quad .$$

Figure 2.1 indicates the number of $l^{\pm}fX$ events necessary to detect a given asymmetry with three or five standard deviations.[4] The total number of $B\bar{B}$ events is obtained by

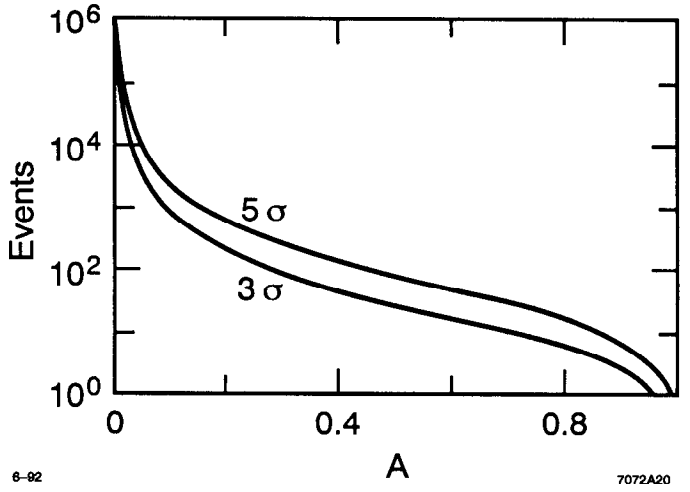

Figure 2.1. The number of lfX events necessary to detect a given asymmetry A, with 3 or 5 standard deviations. The curves are only valid for $A \leq 0.9$.

taking into account the branching ratios and the efficiencies for detecting the decaying channels. The complications due to the mistagging of the decay leptons are discussed in Appendix B.

Table 2 gives estimates of B branching ratios (Br) and CP violation effects for some decay channels.[3] In this Table, CP violation is given by sin 2ϕ where

$$A \simeq \frac{x_{d,s}}{1+x_{d,s}^2} \sin 2\phi \ ,$$

$x_{d,s}$ being the mixing parameters of the $B_{d,s}^0$ mesons. We also show some examples of $B_s^0 \rightarrow f$ decays where no CP violation is expected in the framework of the standard model.[5] This happens when $f = \bar{f}$, and $b \rightarrow c$ (or $\bar{b} \rightarrow \bar{c}$). In any case, the $B_s^0, \bar{B}_s^0 \rightarrow lfX$ channel has to be measured in order to see if sources from the nonstandard model are responsible for CP violation. Note that the study of B_s^0 decays will be particularly suitable at the SSC since the $pp \rightarrow b\bar{b}X$ cross section is expected to be large (Table 1), yielding $\sim 10^{11}$ B_s^0 (and/or $\bar{B}_s^0$) per one year of running.

2.2 - Unequal B and $\bar{B}$ production

One difficulty expected in pp interactions is that B and $\bar{B}$ may not be produced in equal amounts. It was suggested[6-8] that there are essentially two mechanisms which may lead to unequal amounts of produced B and $\bar{B}$ [$N(B)$ and $N(\bar{B})$]. The first one involves the combination of produced b or $\bar{b}$ with the quarks of the incident beam particles. This could correspond to b quarks emitted with

Table 2 - Estimation of the branching ratios Br and the CP violation parameter $\sin 2\phi$ ($A \simeq x_{d,s}/(1+x_{d,s}^2)\ \sin 2\phi$) for some B^0 decays.[3] In the first case, the $J/\psi \to l^+l^-$ branching ratio is contained in Br. For the $\sin 2\phi = 0$ case, see Ref. 5.

	Br	$\sin 2\phi$
$B_d^0 \to J/\psi K_s^0$	$\sim 4 \times 10^{-4}$	0.1–0.6
$B_d^0 \to D^+D^-$	$\sim 10^{-3}$	0.1–0.6
$B_d^0 \to \pi^+\pi^-$	$\sim 10^{-5}$	0.2–0.8
$B_d^0 \to \rho^0 K_s^0$	5×10^{-7}–5×10^{-6}	0.2–0.8
$B_s^0 \to D_s^+ D_s^-$	$\sim 2 \times 10^{-2}$	0
$B_s^0 \to J/\psi\phi$	$\sim 5 \times 10^{-3}$	0
$B_s^0 \to \rho^0 K_s^0$	10^{-5}–10^{-4}	0.1–0.8
$B_s^0 \to K^+K^-$	$\sim 5 \times 10^{-7}$	0.3–0.8

small transverse momentum[7-8] ($p_T \leq 5$ GeV/c). In this case one expects that $N(B^+)/N(B^-), N(B_d^0)/N(\bar{B}_d^0) > 1$. The second mechanism is expected to be observed for b quarks with large p_T ($p_T \gg 5$ GeV/c). In this region the structure functions will increase the production of u quarks. Then the process $g \to b\bar{b}$ may lead to additionnal $B^+ \equiv \bar{b}u$ production. This effect is expected to be smaller than the first one.[8]

In order to have an estimate of the $N(B)/N(\bar{B})$ ratios, we used the PYTHIA Monte Carlo program.[9] For the SSC ($\sqrt{s} = 40$ TeV) or LHC ($\sqrt{s} = 16$ TeV) center-of-mass energies, we generated about 10^6 $pp \to b\bar{b}X$ events in order to have small statistical errors on the $N(B)/N(\bar{B})$ ratios (Table 3). With fixed targets ($\sqrt{s} = 0.19,\ 0.12$, for the SSC and LHC beam-proton collisions, respectively), only $\sim 5 \times 10^5$ pp events were generated. For all the estimates we used events where only one $b\bar{b}$ pair was produced.

To reduce the event generation time, we did not use gluon "splitting" in the PYTHIA program. This means that we neglect the two gluons produced in the final state, where one of them fragments into a $b\bar{b}$ system. We implicitely assume that the p_T distribution of the B mesons is not changed by neglecting the "splitting" graph. To verify our estimates we also generate $\sim 8 \times 10^5$ events by taking into account gluon "splitting" resulting in only $\sim 3.7 \times 10^4$ $b\bar{b}$ events at $\sqrt{s} = 40$ TeV. The value of the ratio $N(B)/N(\bar{B}) = 1.013 \pm 0.010$ is not in contradiction with our result given in Table 3.

Table 3 - The ratios of the the number of B and $\bar{B}$ $(B/\bar{B})$ produced in pp interactions estimated with the PYTHIA Monte Carlo programs.

	$\sqrt{s}$, TeV	PYTHIA
$B/\bar{B}$	0.12	1.021 ± 0.001
B^+/B^-	-	1.129 ± 0.002
$B_d^0/\bar{B}_d^0$	-	0.992 ± 0.002
$B_s^0/\bar{B}_s^0$	-	0.757 ± 0.004
$B/\bar{B}$	0.19	1.023 ± 0.001
B^+/B^-	-	1.104 ± 0.002
$B_d^0/\bar{B}_d^0$	-	1.005 ± 0.002
$B_s^0/\bar{B}_s^0$	-	0.812 ± 0.004
$B/\bar{B}$	16.0	1.004 ± 0.001
B^+/B^-	-	1.013 ± 0.002
$B_d^0/\bar{B}_d^0$	-	1.002 ± 0.002
$B_s^0/\bar{B}_s^0$	-	0.980 ± 0.003
$B/\bar{B}$	40.0	1.003 ± 0.001
B^+/B^-	-	1.009 ± 0.002
$B_d^0/\bar{B}_d^0$	-	1.001 ± 0.002
$B_s^0/\bar{B}_s^0$	-	0.993 ± 0.003

We also give, in Table 3, the $N(B)/N(\bar{B})$ ratios for different types of B mesons. One sees from this table that

$$\frac{N(B^+)}{N(B^-)} \geq \frac{N(B_d^0)}{N(\bar{B}_d^0)} \geq \frac{N(B_s^0)}{N(\bar{B}_s^0)} \quad .$$

We also note that $N(B_s^0)/N(\bar{B}_s^0)$ tends to be smaller than one, in contrast to the other cases. Moreover, the deviation of $N(B)/N(\bar{B})$ from the value one decreases when $\sqrt{s}$ increases. Practically, the B and $\bar{B}$ appear to be produced in equal amounts at the SSC center-of-mass energy. In Table 4 we present the various $N(B)/N(\bar{B})$ ratios in different B transverse momentum intervals using the PYTHIA program. We see that in most cases $N(B)/N(\bar{B})$ tends to increase with p_T.

For the present estimates we do not use the ISAJET program[9], where the independent fragmentation processes lead to $N(B)/N(\bar{B}) = 1$ (this was verified by generating ISAJET events at the various $\sqrt{s}$ cases).

2.3 - Discussion

The study of the time-dependent rate of $B^0 \rightarrow f$ decay can also be utilized in searching for CP violation effects.[10] In this case the investigation will (practically) not depend on the relative amounts of B and $\bar{B}$ production.[6] Experimentally, however, the time evolution measurement of the $B^0 \rightarrow f$ decay will be difficult.[6] One must also emphasize that unequal amounts of B and $\bar{B}$ production could also lead to some advantages.[5] Without any tagging, the time-dependent rate of $B^0_{d,s} \rightarrow f$ and $\bar{B}^0_{d,s} \rightarrow f$ can be written

$$\frac{dN(B^0_{d,s} \rightarrow f)}{d\tau_{d,s}} + \frac{dN(\bar{B}^0_{d,s} \rightarrow f)}{d\tau_{d,s}} \propto [1 - \bar{A}\, n\, \sin(x_{d,s}\tau_{d,s})]$$

$$\bar{A} = \frac{N(B^0_{d,s}) - N(\bar{B}^0_{d,s})}{N(B^0_{d,s}) + N(\bar{B}^0_{d,s})} .$$

Here $\tau_{d,s}$ is the meson decay time in lifetime units expressed in the $B^0_{d,s}$ rest frame, whereas $n \equiv \sin 2\phi$ is the CP violation parameter. Thus, the observation of an oscillation in the time evolution of the B^0 and $\bar{B}^0$ decay would indicate CP violation. However, such an effect will be difficult to measure for $\bar{A} \times n \leq 0.03$ (Ref. 6). Cuts on the B transverse momentum might be useful to increase $\bar{A}$ (see Table 4). As no tagging procedure is needed for this method, one could eventually consider larger luminosities ($L \simeq 10^{33}$ cm^{-2} s^{-1}) in order to increase the statistics. In any case, further studies must be made in order to evaluate the usefulness of the above effects.

The $N(B)/N(\bar{B})$ ratio is important for searching in CP violation in pp interactions. Based on PYTHIA, the amounts of B and $\bar{B}$ appear to be almost equal at $\sqrt{s} = 40$ TeV. Clearly, the $N(B)/N(\bar{B})$ ratios have to be measured by using decay channels where CP violation effects are not expected. The comparison of $B^{\pm} \rightarrow D^{*\pm}(2010)\,\pi^+\pi^-\pi^0$, $D^0(\bar{D}^0)\rho^{\pm}$, $J/\psi K^{\pm}$ events could, for instance, give an estimate of B^+/B^-. In any case, the $B/\bar{B}$ measurements would require a large number of events. We also notice that B^0_s decays could be measured easily, as some of their branching ratios are expected to be large. The search for CP violation in some of these cases would allow a test of the standard model.

Table 4 - The ratios of the the number of B and $\bar{B}$ ($B/\bar{B}$) estimated with PYTHIA in various p_T (GeV/c) ranges of the B mesons.

	$\sqrt{s}$, TeV	$0 < p_T \leq 2.5$	$2.5 < p_T \leq 5$	$5 < p_T \leq 10$	$p_T \geq 10$
$B/\bar{B}$	0.12	0.990 ± 0.002	1.029 ± 0.002	1.080 ± 0.004	1.079 ± 0.019
B^+/B^-	-	1.109 ± 0.003	1.134 ± 0.003	1.167 ± 0.005	1.251 ± 0.028
$B^0_d/\bar{B}^0_d$	-	0.957 ± 0.004	0.999 ± 0.003	1.061 ± 0.006	1.000 ± 0.028
$B^0_s/\bar{B}^0_s$	-	0.701 ± 0.007	0.773 ± 0.007	0.854 ± 0.011	0.844 ± 0.053
$B/\bar{B}$	0.19	0.990 ± 0.002	1.025 ± 0.002	1.074 ± 0.003	1.058 ± 0.012
B^+/B^-	-	1.080 ± 0.004	1.105 ± 0.003	1.145 ± 0.005	1.091 ± 0.018
$B^0_d/\bar{B}^0_d$	-	0.967 ± 0.004	1.008 ± 0.003	1.060 ± 0.05	1.071 ± 0.018
$B^0_s/\bar{B}^0_s$	-	0.761 ± 0.007	0.813 ± 0.007	0.890 ± 0.009	0.912 ± 0.034
$B/\bar{B}$	16.0	0.988 ± 0.003	1.002 ± 0.002	1.009 ± 0.002	1.011 ± 0.003
B^+/B^-	-	0.997 ± 0.004	1.013 ± 0.003	1.022 ± 0.003	1.011 ± 0.004
$B^0_d/\bar{B}^0_d$	-	0.987 ± 0.004	1.000 ± 0.003	1.005 ± 0.003	1.014 ± 0.004
$B^0_s/\bar{B}^0_s$	-	0.964 ± 0.007	0.973 ± 0.005	0.983 ± 0.005	1.000 ± 0.007
$B/\bar{B}$	40.0	0.995 ± 0.003	1.000 ± 0.009	1.09 ± 0.002	1.004 ± 0.002
B^+/B^-	-	1.000 ± 0.004	1.009 ± 0.003	1.016 ± 0.003	1.000 ± 0.004
$B^0_d/\bar{B}^0_d$	-	0.996 ± 0.004	0.994 ± 0.003	1.004 ± 0.003	1.006 ± 0.004
$B^0_s/\bar{B}^0_s$	-	0.978 ± 0.008	0.984 ± 0.006	0.997 ± 0.005	1.010 ± 0.006

3 - B mesons in the central region

3.1 - Remarks about the central region

At $\sqrt{s} = 40$ TeV, the $pp \to b\bar{b}X$ cross section is predicted to be large ($\sigma(b\bar{b}) \simeq 500$ μb , see Table 1) and could thus give access to investigation of B-physics. In the usual collider projects,[11,12] charged particles will only be measured if their (laboratory) emission angle is larger than $\sim 10°$ (corresponding to $\eta \leq |2.4|$). Even in this case, the number of $pp \to b\bar{b}X$ is still large. This is shown in Table 5 which compares the number of $B\bar{B}X$ events obtained in one year of running where the charged particles from B decays are emitted with $\Theta > 10°$ and with $1 \leq \Theta \leq 10°$ (the forward cone, see below). We also see that the average charged multiplicity $\langle n \rangle$ for $b\bar{b}X$ final states is not too large.

Table 5 - The number of $b\bar{b}X$ events in one year of running for various cases. The average charged multiplicity ($< n >$) is also indicated for $pp \rightarrow b\bar{b}X$ events.

	$\langle n \rangle$	$N(b\bar{b})/10^7$ s
No cut	-	$\sim 5 \times 10^{11}$
$\Theta > 10°$	~ 52	$\sim 2.8 \times 10^{11}$
$1 \geq \Theta \geq 10°$	~ 30	$\sim 5 \times 10^{10}$

In future SSC experiments,[11,12] the search for Higgs is also based on the detection of muons having large transverse momentum or momentum and emitted with $|\eta| \leq 2.4$. This type of trigger could also be sensitive to some B decay channels. In particular, one could investigate the possibility of detecting the decay $B_d^0 \rightarrow J/\psi K_s^0$ with $J/\psi \rightarrow \mu^+\mu^-$ and $K_s^0 \rightarrow \pi^+\pi^-$.

3.2 - The $B_d^0 \rightarrow J/\psi K_s^0$ channel

The study of this channel is useful in the search for CP violation in the $B_d^0, \bar{B}_d^0 \rightarrow J/\psi K_s^0$ decay. The branching ratio used is $\sim 1.9 \times 10^{-5}$ with $J/\psi \rightarrow \mu^+\mu^-$ and $K_s^0 \rightarrow \pi^+\pi^-$. The associated beauty hadron is tagged with the $B, \bar{\Lambda}_b \rightarrow \mu^+ X$ and $\bar{B}, \Lambda_b \rightarrow \mu^- X$ decays. Figure 3.1 presents the detection efficiency of the $pp \rightarrow B\bar{B}X \rightarrow 3\,\mu X$ reactions by applying transverse momentum or momentum cuts on 1, 2 or 3 muons calculated with the ISAJET program. For these calculations, we assume that the K_s^0 has to decay in a cylindrical volume around the beam line, having a radius $R < 1$ m.

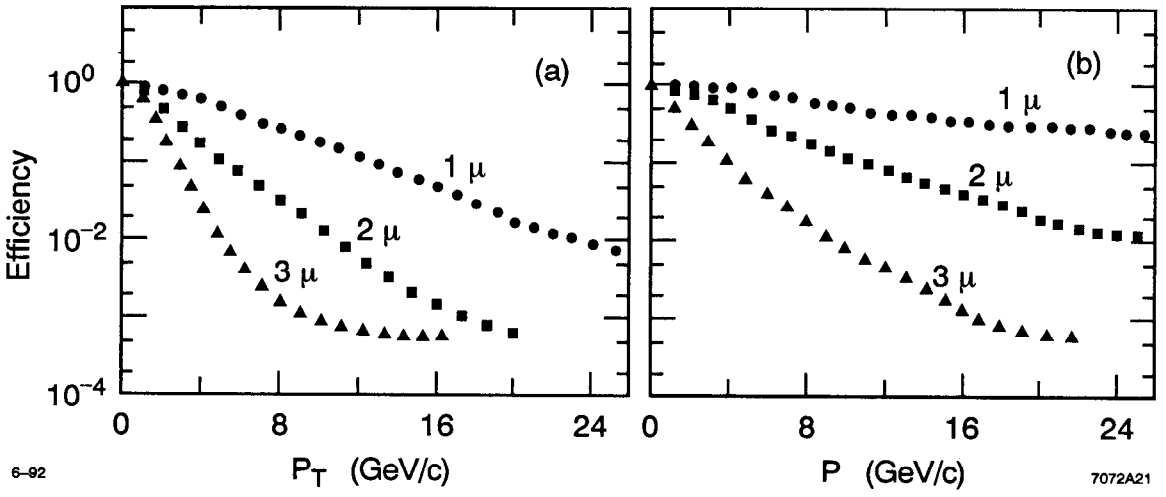

Figure 3.1. The detection efficiency of $pp \rightarrow 3\ \mu X$ for a p_T cut (a) or a p cut (b) on 1, 2, or 3 muons.

Table 6 - Acceptance for the beauty hadrons decaying into $\psi K_s^0 \mu X$ where the charged particles are emitted in the $|\eta| \leq 2.4$ region. We assume that $(b \to B_d^0)/(b \to \text{all}) = (\bar{b} \to \bar{B}_d^0)/(\bar{b} \to \text{all}) = 0.38$. Here, $\Theta(\psi, K_s^0)$ represents the opening angle between the J/ψ and the K_s^0.

$(b \to B_d^0)$ and/or $(\bar{b} \to \bar{B}_d^0)$ production	0.62
$\text{Br}(B_d^0 \to \psi K_s^0,\ \psi \to \mu^+\mu^-,\ K_s^0 \to \pi^+\pi^-)$	1.9×10^{-5}
$\text{Br}(b \to \mu X)$	0.12
$3\,\mu$ with $\|\eta\| \leq 2.5$	0.34
$3\,\mu$ with $p > 5$ GeV/c	8.4×10^{-2}
$3\,\mu$ with $p_T > 1.5$ GeV/c	0.88
K_s^0 with $\|\eta\| \leq 2.5$	0.91
K_s^0 with $p_T > 1$ GeV/c	0.87
K_s^0 decaying in $R < 1$ m	0.81
$\cos\Theta(\psi, K_s^0) > 0.9$	0.77
Efficiency of tracking and μ identification	$(0.6)^3$
Total efficiency	$\sim 3.7 \times 10^{-9}$

To get an estimate of the number of $J/\psi K_s^0 \mu X \to 3\,\mu\pi^+\pi^- X$ events in one year, we used the efficiencies given in Table 6. For the present discussion we used an overall efficiency of 0.6 for tracking and identifying a muon. This value is an estimate often used in the SDC project discussion. With a luminosity of $L = 10^{32}$ cm^{-2} s^{-1}, a cross section of $\sigma(b\bar{b}) \simeq 500$ μb, and the total efficiency given in Table 6 (3.7×10^{-9}), one expects to obtain $\sim 1850\ \mu^+\mu^-\mu^\pm K_s^0 X$ events per one year of running. As can be seen from Fig. 3.1, a $p_T > 5$ GeV/c cut for the $3\,\mu$ (without momentum cuts) will decrease the efficiency, leading to only ~ 250 events per year. Note that for the $3\,\mu\pi^+\pi^- X$ final state, one could perhaps envision larger luminosities ($L > 10^{32}$ cm^{-2} s^{-1}). This is because the longitudinal dimension of the interaction diamond ($\sigma_z \simeq 5$ cm) may allow us to separate some of the double interactions per bunch crossing. This might decrease the wrong identification of the muon tag.

We also estimate the background in the identification of the $pp \to 3\,\mu K_s^0 X$ sample. The background muons could be produced by the $b \to \mu$, $c \to \mu$ processes, and from the $\pi^\pm \to \mu^\pm\nu$ and $K^\pm \to \mu^\pm\nu$ decays. For direct charm production, we use the following cross section ratio: $\sigma(pp \to c\bar{c}X)/\sigma(pp \to b\bar{b}X) \simeq 4$. The background was estimated by using generated events having a $\mu^+\mu^-$ combination yielding the J/ψ mass with a mass resolution of ± 50 MeV and where the reconstructed J/ψ with a K_s^0

in the event gives the B mass (within ± 50 MeV). An additional background is due to real J/ψ that are not produced by the $B_d^0 \rightarrow J/\psi K_s^0$ decay channel. We assume that these J/ψs are essentially due to direct or indirect decay of the B meson ($B \rightarrow J/\psi X$ and $B \rightarrow \chi_c X$ with $\chi_c \rightarrow J/\psi X'$), yielding a cross section of $\sigma(pp \rightarrow J/\psi X) \sim 11$ μb. The direct J/ψ or χ_c production were not taken into account as they decay near the interaction point. With the above assumptions, the signal-to-background ratio is S/B $\simeq 1.2$.

Note that an asymmetry parameter A used for measuring CP violation will be decreased by a factor of S/(S+B)~ 0.6. In order to see the limit of the measurement of the CP violation parameter ($\sin 2\phi$), one has also to take into account the dilution effect appearing in the muon tagging. Appendix B suggests a somewhat different method[13] for estimating the dilution factor[14] related to the $B \rightarrow \mu X$ tagging. In this case, the asymmetry parameter is related to the CP violation parameter ($A = D \times \sin 2\phi$) with a value of $D \simeq 0.13$. For this calculation, unknown B, $\bar{\Lambda}$ branching ratios have been estimated, while punchthrough and muons from π and K decays were not taken into account as they depend on the detector. Kinematic cuts could certainly increase D, but will also decrease the number of events. In any case, detailed investigations have to be made for a given experiment.

4 - *B* mesons in the forward/backward region

4.1 - General remarks

Because of the rather flat rapidity distribution of the particles produced at $\sqrt{s} = 40$ GeV (Fig. 4.1 obtained with a Monte Carlo calculation), the angular distribution of the B mesons is strongly peaked along the beam direction ($dN/\cos\Theta_B \sim 1/\sin^2\Theta_B \; dN/\eta$, where N is the number of events and Θ_B the B emission angle). A forward/backward detector will thus measure a significant fraction of the Bs produced in pp interactions.

In order to evaluate the sensitivity of a forward/backward experiment, we will consider the following decay channels:

$$B_d^0, \bar{B}_d^0 \rightarrow J/\psi K_s^0 \, ,$$

$$B_s^0, \bar{B}_s^0 \rightarrow \mu^+\mu^- \, .$$

The first decay allows the comparison of a forward/backward experiment and a central one. The $B_s^0, \bar{B}_s^0 \rightarrow \mu^+\mu^-$ decay channel is sensitive to deviations from the standard model[15] and could also give information about B_s^0 mixing.[16] As discussed below, a measurement of this branching ratio could be attempted with events where the B_s^0s have large momentum.

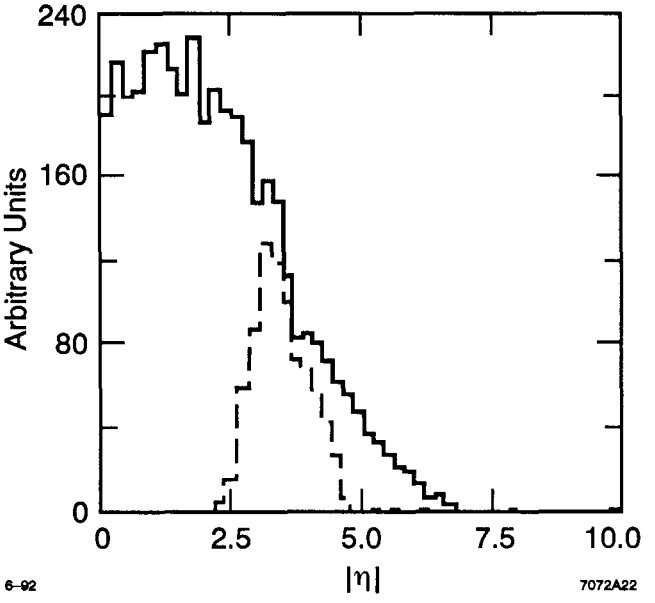

Figure 4.1. The pseudorapidity ($|\eta|$) distribution of the B meson produced in pp interactions at $\sqrt{s}$ = 40 TeV (full line). The same distribution (dashed line) where the$B$ decay tracks are emitted in the $1 \leq \Theta \leq 10°$ cone.

Let us first discuss the general features of the B and $\bar{B}$ production obtained with the PYTHIA Monte Carlo program[9] Figure 4.2 shows the $B\bar{B}$ opening angle, $\Theta(B\bar{B})$. One sees that a large number of $B\bar{B}$ events have a small $\Theta(B\bar{B})$ angle. For small Θ_B emission angle, most of the Bs and $\bar{B}$s are emitted with a small opening angle (see for instance Ref. 4). This means that most of the Bs and $\bar{B}$s tend to be emitted in the same forward (or backward) direction.

Figure 4.3 presents the average B momentum ($\langle p_B \rangle$) as a function of $\Theta_{\max}$. Here $\Theta_{\max}$ is the maximum Θ angle of the charged B decay particles with respect to the beam line. In this figure a minimum emission angle of $\Theta_{\min} = 1°$ is used in the Monte Carlo calculation to take into account the beam-pipe cut. For the present discussion we will only consider the so-called forward cone, where $1 \leq \Theta \leq 10°$. We see from Fig. 4.3 that $\langle p_B \rangle \sim 300$ GeV/c whereas the momentum distribution of the charged tracks is given in Fig. 4.4. These rather large values might facilitate the B reconstruction and the identification of events where the tagged $B \rightarrow \mu X$ channels have muons with large momentum. This could facilitate the triggering. Note that the large $\langle p_B \rangle \sim 300$ GeV/c is comparable to the fixed target case[17] ($\langle p_B \rangle \sim 445$ GeV/c). In both cases $\langle p_B \rangle$ is larger than the value expected in a collider experiment where $|\eta| < 2.5$ ($\langle p_B \rangle \sim 23$ GeV/c).

In Fig. 4.5 we present the efficiency for obtaining B mesons in the forward cone as a function of n, the number of B decay tracks (full line). We also indicate the

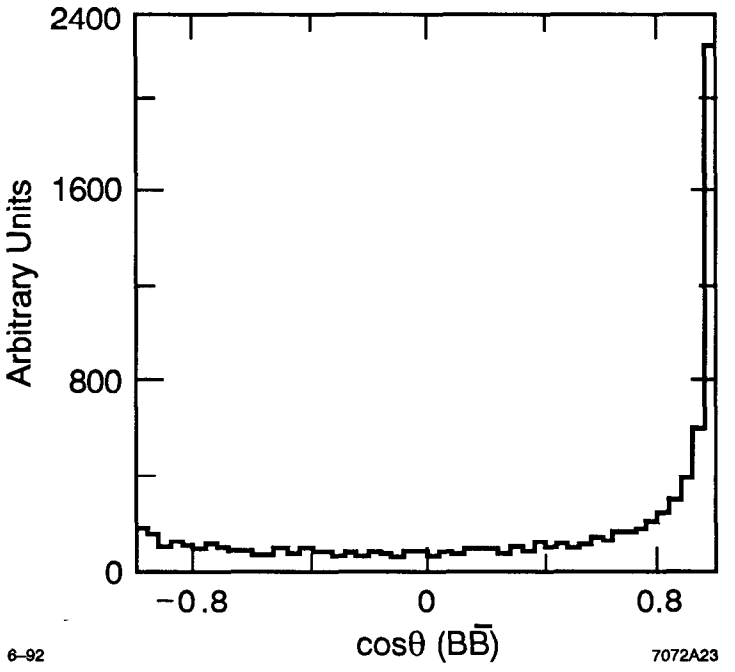

Figure 4.2. The $\cos\Theta(B\bar{B})$ at $\sqrt{s}$ = 40 TeV, $\Theta(B\bar{B})$ being the $B\bar{b}$ opening angle (obtained with the PYTHIA Monte Carlo program).

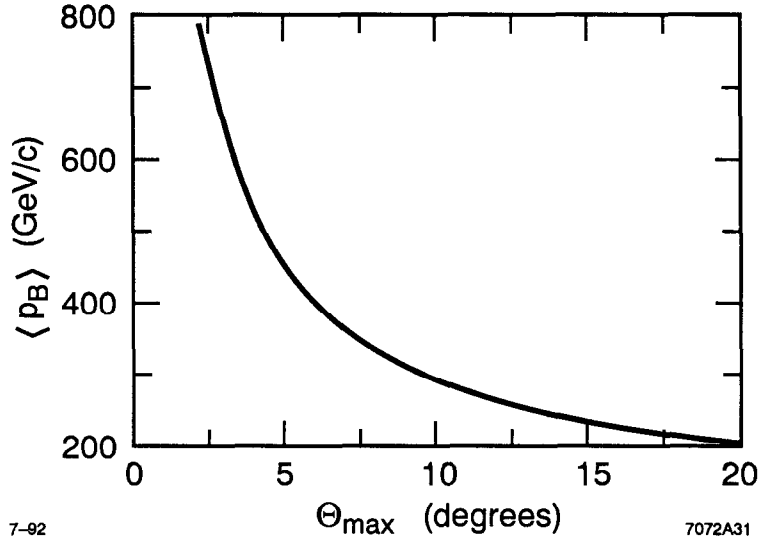

Figure 4.3. The average B momentum ($\langle p_B \rangle$) as a function of $\Theta_{\max}$. Here, $\Theta_{\max}$ is the maximum accepted angle for the charged B decay tracks. The Monte Carlo calculation was made with a minimum angle of 1°.

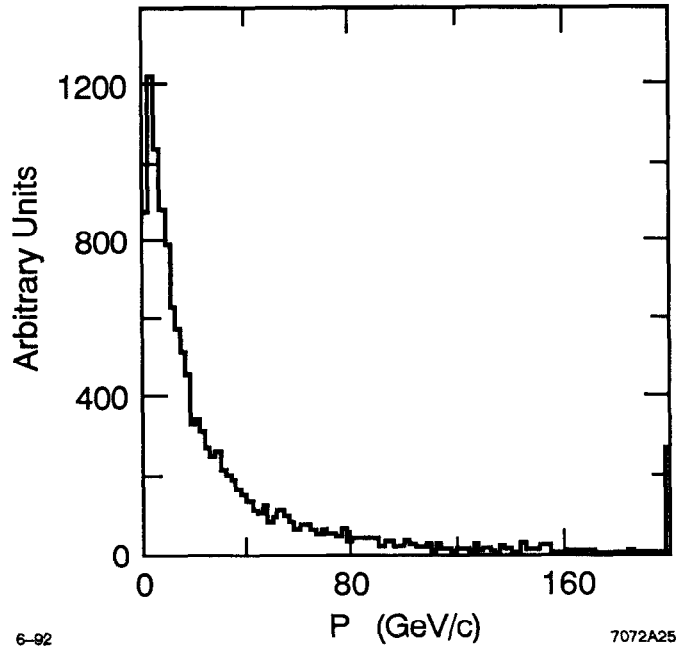

Figure 4.4. Momentum distribution of the B decay tracks emitted with $1 \leq \Theta \leq 10°$.

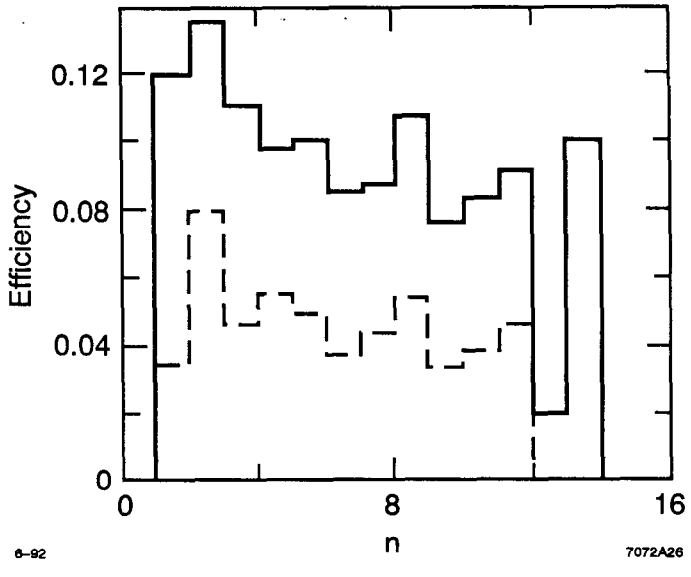

Figure 4.5. The efficiency of detecting B mesons in the forward cone as a function of n, the number of B decay tracks (full line). The dashed line is the efficiency where, in addition, the μ due to the associated $B\bar{B} \rightarrow \mu X$ decay enters into the cone.

Table 7 - Acceptance for the beauty hadrons decaying into $\psi K_s^0 \mu X$. Here we consider the cases where the $3\,\mu$, the π^+ and π^- are emitted in the forward direction ($1 \leq \Theta \leq 10°$, one side only).

$(b \rightarrow B_d^0)$ and/or $(\bar{b} \rightarrow \bar{B}_d^0)$ production	0.62
$\mathrm{Br}(B_d^0 \rightarrow \psi K_s^0, \quad \psi \rightarrow \mu^+\mu^-, \quad K_s^0 \rightarrow \pi^+\pi^-)$	1.9×10^{-5}
$\mathrm{Br}(b \rightarrow \mu X)$	0.12
$3\,\mu$ with $1 \leq \Theta \leq 10°$	4.5×10^{-2}
$3\,\mu$ with $p > 8$ GeV/c	0.77
$3\,\mu$ with $p_T > 1.5$ GeV/c	0.28
K_s^0 with $1 \leq \Theta \leq 10°$	0.85
K_s^0 decaying with $\bar{l} < 5$ m	0.80
Efficiency of tracking and μ identification	0.8
Total efficiency	7.4×10^{-9}

efficiency obtained if, in addition, the μ tag of the associated B or $\bar{\Lambda}_b$ ($\bar{B}$ or Λ_b) enters into the same cone (dashed line). We see that the efficiencies do not depend strongly on n.

4.2 - The $B_d^0 \rightarrow J/\psi K_s^0$ channel

Before discussing the properties of a forward spectrometer, let us estimate the efficiencies for detecting the $J/\psi K_s^0$ events. Here we will consider muons having a momentum larger than 8 GeV/c and $p_T > 1.5$ GeV/c. Table 7 gives the efficiencies for events where the $3\,\mu$ and the $\pi^{\pm}$ from the K_s^0 decay are emitted in the forward direction. We assume that the K_s^0 can decay in a distance to the interaction point of $\bar{l} \leq 5\ m$. The efficiency given in Table 7 corresponds to $\sim$ 3700 events, about two times larger than the prediction obtained in Section 3 for the central region. Here, however, the background is larger as one obtains an estimate of S/B $\sim$ 0.3. Taking into account a mass resolution of $\pm$25 MeV (instead of $\pm$50 MeV obtained in the example discussed below in Section 4.4, S/B $\sim$ 1.2. In any case, detailed investigations have to be made in order to evaluate the possibility of decreasing the background.

4.3 - The $B_s^0 \rightarrow \mu^+\mu^-$ decay

Theoretically, $\mathrm{Br}(B_s^0 \rightarrow \mu^+\mu^-)$ is estimated to be small, namely $\sim 10^{-9}$ (Ref. 15). Therefore, the essential difficulty in identifying these events will be due to the large backgrounds. The dimuon background can be due to the following processes:

$$b\bar{b} \rightarrow \mu^+\mu^- \ , \qquad b\bar{b} \rightarrow c\bar{c} \rightarrow \mu^+\mu^- \ , \qquad c\bar{c} \rightarrow \mu^+\mu^- \ , \qquad \text{Drell-Yan } \mu \text{ pair} \ ,$$

$$\text{and } \pi \text{ and/or } K \text{ decays into } \mu \ .$$

Let us roughly estimate the signal-to-background ratio (S/B) expected in the $B_s^0 \rightarrow \mu^+\mu^-$ decay channel. For the influence of the Drell-Yan process we used the PAPAGENO Monte Carlo program,[18] whereas for the other cases we utilized the PYTHIA program. Based on these calculations, we noticed that the background can be decreased by considering only charged particles having a momentum $p > 5$ GeV/c and a transverse momentum $p_T > 1$ GeV/c. The momentum cuts essentially decrease the contribution of muons due to π and K decays while the $p_T > 1$ GeV/c cut decreases the background due to the processes $b\bar{b} \rightarrow \mu^+\mu^-$ and $b\bar{b} \rightarrow c\bar{c} \rightarrow \mu^+\mu^-$.

Thus, with $1 \leq \Theta \leq 10°$, $p > 5$ GeV/c and $p_T > 1$ GeV/c, one obtains S/B $\simeq 7.6 \times 10^{-5}$. We assumed that the B_s^0 (or $\bar{B}_s^0$) production rate is 0.14 with respect to all particles containing a b (or a $\bar{b}$) quark. A background rejection factor of at least $\sim 4.8 \times 10^4$ is needed to obtain a workable S/B ~ 1 ratio. This means that the detector must have μ detection and B_s^0 vertex reconstruction adequate to obtain this level of background rejection.

4.4 - A forward spectrometer concept

An illustrative example of a forward spectrometer (see Fig. 4.6) is discussed here (see also Refs. 19 and 20). The vertex detector is comprised of silicon hybrid pixel detectors described in Appendix C, while the geometry of the vertex detector is described in Appendix D. A dipole magnet (20 KG) has been used to measure the momentum of the B decay tracks, and particle identification of these decay secondaries is accomplished with a Cherenkov Ring Imaging Detector described in Appendix E. Appendix F describes the muon counters and a number of triggering possibilities. The proposed geometry enables one to detect and identify charged tracks emitted within the forward cone ($1 < \Theta < 10°$), corresponding to $2.4 < |\eta| < 4.7$.

A number of issues must, of course, be addressed:

- effects of radiation damage on the vertex detector,
- geometry of the beam pipe,
- reconstruction of the primary interaction vertex,
- spatial resolution of the displaced vertex,
- triggering,
- effects of the dipole on the collider,
- momentum and mass resolution.

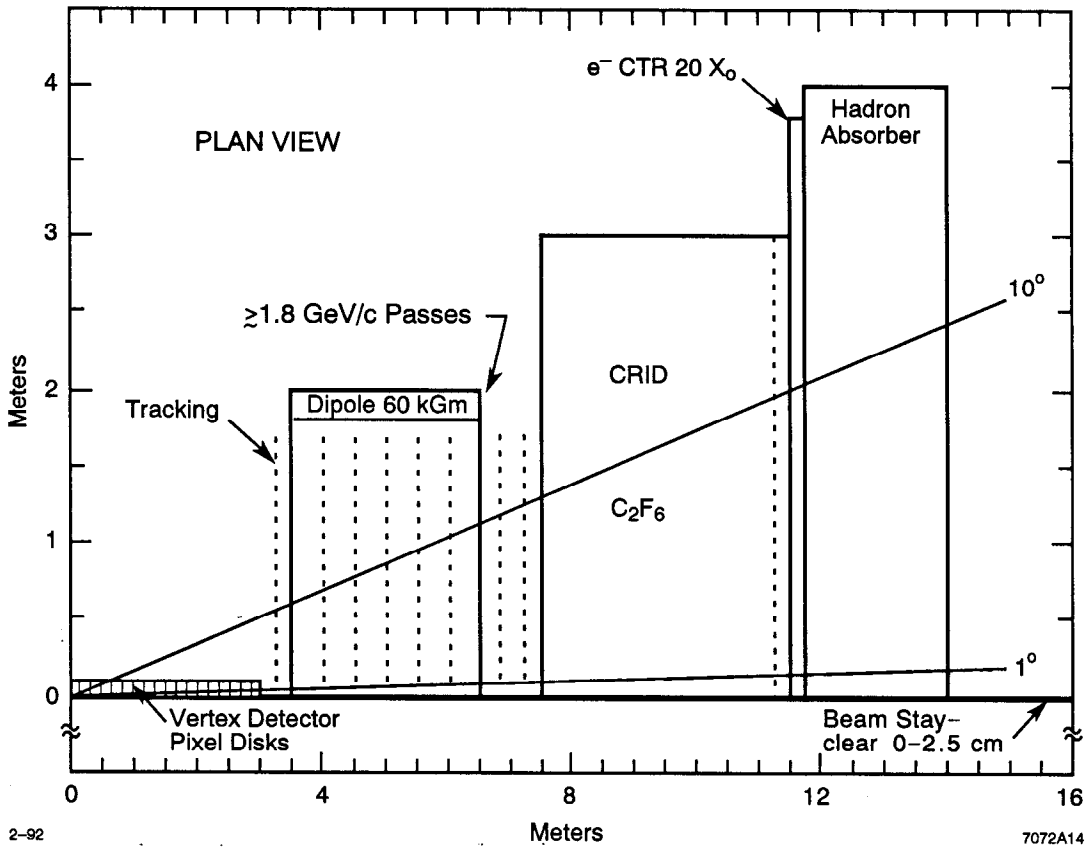

Figure 4.6. An illustrative example of a forward spectrometer, highlighting its main features. The muon detector is not shown.

Radiation at small radii is known to be severe.[21] At a radius of 2 cm from the beam line, a dose rate of 10 MRad per year is expected with a luminosity $L = 10^{33}$ cm^{-2} s^{-1}. The forward spectrometer needs a luminosity $L = 10^{32}$ cm^{-2} s^{-1}, thus decreasing the radiation level. The design goal for the pixel detector hybrids is to harden them to 10 MRad. For added safety, the present vertex detector design calls for the minimum radius R_{min} to be 2.5 cm.

There are many beam pipe designs for forward physics and the selection of the optimum design will have to await detailed Monte Carlo calculations. In this exercise, a conical design shown in Fig. D.1 has been selected that limits the material placed in the path of the B decay secondaries to a 0.5 mm thick membrane of beryllium placed perpendicular to the trajectories of interest.

The decay vertex detector is comprised of a series of 13 disks placed perpendicular to the beam line. Each hybrid placed on these disks is envisioned to be 1 cm square, having pixels which are 50 μm $\times$ 150 μm. For the present, we impose the condition that all tracks must pass through at least four detector disks. Later Monte Carlo

calculations may find that this is too conservative for the two dimensional readout structure proposed.

The minimum detection angle $\Theta_{\min}$ for the B decay tracks, and the minimum radius $R_{\min}$ result in a minimum longitudinal length of the vertex detector $L\,(\mathrm{cm}) > R_{\min}/\tan(\Theta_{\min})$ or 143 cm. Our chosen geometry is a bit longer (300 cm), to account for the finite size of the interacting bunches, to allow a long enough measurement lever arm to retain spatial resolution for the most forward angles, and to allow for our present lack of a detailed simulation.

The necessity of measuring B decay tracks at angles on the order of one degree affects the longitudinal resolution of the decay vertex detector, and complicates the vertex reconstruction of the produced B mesons. The transverse resolution of the vertex detector is a function of the perpendicular distance of the track from the beam line and its transverse momentum. The transverse momentum of B decay tracks in this spectrometer is $\sim$ 2 GeV/c, nearly identical to that expected in low η collider experiments, resulting in nearly identical impact parameters as well. For tracks emanating from all decay sources, for example, Fig. D.3 presents the transverse and longitudinal resolution as a function of emission angle Θ (and transverse momentum p_T) for tracks having a total momentum of 13.6 GeV/c. For B decay tracks, typically, the transverse resolution is less than 25 μm and the resolution in the beam direction (z) is better than 350 μm. For these estimates, it is implicitly assumed that the disk alignment is stable to a fraction of the resolution in the transverse plane.

The interaction vertex is identified and reconstructed using charged particles produced in the pp interaction with small $|\eta|$ values (Θ around 90°). A series of three small cylinders, also comprised of hybrid pixel detectors, measures its position. The orientation of the hybrids in this portion of the detector is such that the short dimension of the pixel is along the beam direction. Because of the small size of the SSC beam (radius of about 1.5 μm), one has only to determine the z-position. For each track whose total momentum is greater than 2 GeV/c a resolution of better than 20 μm is obtained.

In this spectrometer design, a gas Ring Imaging Cherenkov Counter is used for particle identification (Fig. 4.6). This counter, using a C_2F_6 gaseous radiator of modest length (about 4 m), allows:

- π/K separation from 3.5–95 GeV/c,
- e/π separation up to 29 GeV/c,
- μ/π separation from 2.6–19 GeV/c,

at the $4\,\sigma$ level. Additional details of this counter are also provided in Appendix E.

A conventional dipole magnet having a field integral of 60 KGauss-meters is proposed as the analyzing magnet. Decay particles having a total momentum of less than 1.8 GeV/c will not exit the magnet. Thus, it is prudent to include in the design a tracking system that measures particle trajectories within, as well as exterior to, the magnet. Appendix G estimates the B-meson mass resolution expected for the type of detector discussed above. Estimates are made for B_d^0 decaying into two ($B_d^0 \to \pi^+\pi^-$) and four ($B_d^0 \to \bar{D}^0 K^* \to 2K^+ 2\pi^-$) charged particles for various detector parameters.

The lepton identifiers, the electron and muon counters, have not been specified yet. Their depth and segmentation must be determined only after careful study. A discussion of triggering and some thoughts on muon counters are presented in Appendix F.

5 - Experiments with fixed targets

5.1 - Advantages and disadvantages

The fixed-target experiments have some advantages, although the center-of-mass energy with the SSC beam is rather small, $\sqrt{s} = 0.19$ TeV. At this center-of-mass energy, the $pp \to b\bar{b}X$ reaction is estimated to be $\sigma(b\bar{b}) \simeq 2$ μb, much smaller[1] than the cross section at the collider (~ 500 μb). Fixed target experiments can be done in two ways, with an external target or with a gas-jet, and they have several advantages, namely:

- the larger momentum of the outgoing tracks leads to better momentum resolution[4] (multiple scattering is decreased),
- the large momentum of the produced Bs allows them to pass through planes of detectors before decaying,
- the high momentum of the leptons coming from the $B \to lX$ decrease triggering difficulties, and
- the lower multiplicity of charged particles will decrease the background for the reconstruction of B mesons ($\langle n \rangle \sim 17$ for pp interactions).

There are also disadvantages, such as:

- the produced particles tend to be emitted with a small angle (with respect to the beam line), complicating the B reconstruction,
- the collimation of the outgoing tracks requires the construction of a vertex detector with a precisions of a few microns,
- the large average particle momentum makes particle identification more difficult, and
- the $\sigma(b\bar{b})$ cross section is small, yielding a large background.

Note that for an external target, the construction of a detector is simplified because plane geometry can be used. In addition, there is no beam pipe obstructing the interaction region.

Let us discuss some aspects related to the background and the charged multiplicity appearing in pA collisions (where A denotes the target nuclear mass number). For a hydrogen target, one has:

$$R(A=1) \;=\; \frac{\sigma(b\bar{b})}{\sigma_{\rm in}} \;\sim\; \frac{1}{21000} \quad .$$

Using $\sigma(b\bar{b}) \sim 2\ \mu$b and an inelastic cross section, $\sigma_{\rm in} = \sigma_T - \sigma_{\rm el} \simeq 41$ mb (Ref. 1), while the elastic cross section, $\sigma_{\rm el} \sim 9$ mb has been roughly estimated by extrapolation of the actual data. The background is expected to be large since in $\sim 2 \times 10^4$ events, there will be only one $\sim b\bar{b}X$ event. Note that this R value is much smaller than the value expected at the SSC collider ($\sim 1/240$, Table 1). By using pA collisions, this ratio increases as the inelastic pA and $pp \rightarrow b\bar{b}X$ cross sections ($\sigma_{\rm in}^A$ and $\sigma^A(b\bar{b})$, respectively) are given by[22]

$$\sigma_{\rm in}^A = \bar{\sigma}_{\rm in}\ A^{\alpha(T)}$$

$$\sigma^A(b\bar{b}) = \bar{\sigma} A^{\alpha(b)} \ .$$

The $\bar{\sigma}_{\rm in}$ and $\alpha(T)$ have been measured[22,23] with p beams. The QCD models predict that $\alpha(b) = 1$ (Ref. 24), although recent experimental results [charm and $\Upsilon(nS)$ production[25,26]] indicate that $\alpha(b)$ could be smaller, but close to one. Experimental results indicate that for charm production, $\bar{\sigma}/\bar{\sigma}_{\rm in} \simeq \sigma(c\bar{c})/\sigma_{\rm in}$ (although $\bar{\sigma}_{\rm in} > \sigma_{\rm in}$). We assume that this type of relation is also valid for $b\bar{b}$ production. One has then:

$$R(A) \;=\; \frac{\sigma^A(b\bar{b})}{\sigma_{\rm in}^A} \;\simeq\; \frac{\sigma(b\bar{b})}{\sigma_{\rm in}} \;\times\; A^{\alpha(b)-\alpha(T)} \quad .$$

Practically, the utilization of a nuclear target will be useful if $\alpha(b) \geq 0.9$.

Note, however, that the average charged multiplicity on a nuclear target, $\langle n(pA)\rangle$, is larger than that obtained in pp interactions, $\langle n\rangle$. The experimental data indicate that[23,27]

$$\frac{\langle n(pA)\rangle}{\langle n\rangle} \;\simeq\; \frac{1+\bar{\nu}}{2} \quad .$$

Here $\bar{\nu} = A\sigma_{\rm in}/\sigma_{\rm in}^A$ is the average number of collisions of the incident particle in the nuclear target.[28] Using $\alpha(T) = 0.72$ (Ref. 23) and $\alpha(b) = 1$, one has

$$\frac{\langle n(pA)\rangle}{\langle n\rangle} \;\leq\; \frac{1+A^{0.28}}{2} \quad .$$

Table 8 - The number of $b\bar{b}$ produced in one year of running ($N(b\bar{b})/y$) and the number of inelastic interactions per second ($N_{\rm int}$/s) for various external targets assuming an external beam of 10^8 p/s. The targets have a length of $\langle l_{\rm int}\rangle/10$ (along the beam interaction). Here $\langle l_{\rm int}\rangle$ and $\langle l_{\rm rad}\rangle$ are the average interaction and radiation length in a given target. We also give $R(A)$, $\langle n(pA)\rangle/\langle n\rangle$ and some $P(m)/P(1)$ ratios. The $P(m)$ represent the probability of having m interactions per bunch crossing.

	Be (A=9)	Si (A=28)	Cu (A=63)	W (A=184)
$\langle l_{\rm int}\rangle$, cm	40.6	45.5	15.0	9.6
$\langle l_{\rm rad}\rangle$, cm	35.2	9.4	1.4	0.35
$N_{\rm int}$/s	9.8×10^6	10^7	1.1×10^7	1.1×10^7
$N(b\bar{b})/y$	8.8×10^9	1.3×10^{10}	2.5×10^{10}	2.3×10^{10}
$P(2)/P(1)$	8×10^{-2}	8.5×10^{-2}	8.5×10^{-2}	9×10^{-2}
$P(3)/P(1)$	1.1×10^{-3}	4.8×10^{-3}	4.8×10^{-3}	6×10^{-3}
$\langle n(pA)\rangle/\langle n\rangle$	1.43	1.77	2.10	2.65
$R(A)$	1/11000	1/8100	1/6400	1/4800

5.2 - External target

The utilization of an external fixed target for studying $pA \to b\bar{b}X$ reactions have been proposed.[17] An external beam of at least 10^8 p/s would be necessary in order to search for CP violation in B decay. The possibility of having an external beam at the SSCL is now under investigation (see Appendix A).

As discussed above, the utilization of targets with large atomic number will lead to an increase of $\sigma^A(b\bar{b})$ and $R(A)$. However, the $\langle l_{\rm int}\rangle/\langle l_{\rm rad}\rangle$ ratio will also increase with A. Here $\langle l_{\rm int}\rangle$ and $\langle l_{\rm rad}\rangle$ are the average interaction and radiation lengths, respectively, of a given target. This implies that an increase in the number of showers in a target may complicate the event analysis. As an example we present in Table 8 the number of $b\bar{b}X$ events obtained in one year ($N(b\bar{b})/y$) and the number of inelastic pp interaction produced per second ($N_{\rm int}$/s) for various targets with a length of $\langle l_{\rm int}\rangle/10$ (along the beam direction). One sees that for all these targets, $N_{\rm int}/s \sim 10^7$ (similar to the collider case, Table 1) while $N(b\bar{b})/y \sim 10^{10}$. This later value is an order of magnitude smaller than that obtained in a central collider. For a forward experiment, $N(b\bar{b})/y$ is similar to the external target examples. In Table 8 we also give the $\langle n(pA)\rangle/\langle n\rangle$ and $R(A)$ values. Assuming that the external beam would have the same time structure as the collider, we also evaluate the $P(2)/P(1)$ and $P(3)/P(1)$) ratios. As defined above, $P(m)$ represents the probability of having

Table 9 - The estimates of $N(b\bar{b})/y$, $\langle n(pA)\rangle/\langle n\rangle$ and $\sigma(b\bar{b})/\sigma_{\rm in}$ for various gas-jet targets having a length of 0.2 cm (along the beam direction) and $P(2)/P(1) = 0.025$. This leads to $N_{\rm int}/{\rm s} = 3.1 \times 10^6$ (and to $P(3)/P(1) = 4\times10^{-4}$) for all cases. For each target the number of atom per cm^3 ($N_{\rm at}/{\rm cm}^3$) and the luminosity (L) are also given.

	H (A=1)	Ar (A=40)	Xe (A=131)
$N_{\rm at}/{\rm cm}^3$	8.1×10^{14}	5.7×10^{13}	2.4×10^{13}
L, cm^{-2} s^{-1}	7.1×10^{31}	5.0×10^{30}	2.1×10^{30}
$N(b\bar{b})/y$	1.4×10^9	3.9×10^9	5.5×10^9
$\langle n(pA)\rangle/\langle n\rangle$	1	1.90	2.46
$\sigma(b\bar{b})/\sigma_{\rm in}$	1/21000	1/7300	1/5200

m interactions per bunch crossing with the fixed target. The $P(2)/P(1)$ values are of the order of 8.5×10^{-2}. In searching for CP violation, this value may be too large if the external beam has a small size (this is different for the collider case where the interacting region has a length of $\sim$ 7 cm along the beam direction).

As the average decay length of the B meson is of the order of $\langle l_B\rangle \sim 3$ cm, the target thickness has to be smaller in order to detect the B decay vertices. For Si and Be, for instance, several foils would be necessary. The fact that the target is made of various plates leads to advantages[17] and also to some disadvantages. For example, a secondary interaction might complicate the measurement of the B decay vertices. For the time being, further investigations[29] are being carried out in order to determine the best target and vertex detector.

5.3 - Gas-jet target

At the SSC, an expression of interest[30] for the utilization of a gas-jet has been presented. The advantages of a point source target have also been discussed. At the SSC such a gas-jet could be placed in a region where the p beam pipes are separated by a distance of $\sim$ 80 cm. Such a distance will facilitate the construction of the target device as well as the spectrometer (for the LHC expression of interest,[31] this distance is considered to be $\sim$ 18 cm). In principle, the interaction of the p beam with a gas-jet target can occur with large luminosities as the beam intensity at the SSC should be $\sim 4.4\times10^{17}$ p/s. However, the luminosity has to be limited in order to avoid multiple interactions per bunch crossing. This is important for a point-source form of target, used to search for CP violation in B decay (decay and tagging). For the following examples we use $P(2)/P(1) = 0.025$. This corresponds to $N_{\rm int}/s \sim 3.1 \times 10^6$, with a target length of 0.2 cm along the beam line, and to $\langle m\rangle \sim 0.05$. Table 9 indicate

the luminosities, and the number of atoms per cm^3 needed for several gas-jet targets. The values of $N(b\bar{b})/y \sim 10^9$ are smaller by a factor of ~ 10 than those estimated for a beam of 10^8 p/s interacting with an external target. In these cases, however, showers produced in the gas-jet are negligible.

6 - Summary

We have discussed several possibilities for studying B physics at the SSC. We began our discussions by considering the search for CP violation in B decay. We considered the complication of unequal amounts of B and $\bar{B}$ production that could appear in pp interactions. Based on actual Monte Carlo programs such effects appear to be negligible at the SSC center-of-mass energy. Experimental possibilities were considered for the following cases:

(1) collider experiments where the charged particles are emitted with pseudorapidities of $|\eta| \leq 2.4$ (the central region);

(2) forward experiments where the charged particles are emitted between 1 and 10°;

(3) experiments where the 20 TeV/c p-beam interacts with fixed targets (external or gas-jet target).

The first two points were compared, using the search for CP violation in the decay of $B_d^0, \bar{B}_d^0 \to J/\psi K_s^0 \to \mu^+\mu^-\pi^+\pi^-$. Here we considered tagging made with the $b, \bar{b} \to \mu X$ semileptonic decay. Thus the number of $pp \to J/\psi K_s^0 \mu X \to 3\,\mu\pi^+\pi^- X$ events were estimated with a luminosity of $L = 10^{32}$ cm^{-2} s^{-1}.

The kinematic cuts used for the central region are given in Table 6. Using, in addition, an efficiency of 0.6 for muon tracking and identification, we obtained a rough estimate of $\sim$ 1850 $3\,\mu\pi^+\pi^- X$ events per year of running. The muon momentum cuts were considered as a triggering possibility for the events. The condition that the effective mass of one $\mu^+\mu^-$ be compatible with the J/ψ mass could also be envisioned for the triggering.

One advantage of forward particle detection is that the B meson will have a large momentum (p_B). In the $1 \leq \Theta \leq 10°$ cone we obtained an average of $\langle p_B \rangle \sim 300$ GeV/c. This large value will simplify triggering and the reconstruction of the B meson. We note that this $\langle p_B \rangle$ is close to that expected in an experiment with a fixed target ($\langle p_B \rangle \sim 445$ GeV/c in Ref. 17). One must also remember that the cross section ratio $\sigma(b\bar{b})/\sigma_{\rm in} \sim 1/240$ is much larger than the values obtained with a fixed target (for instance one has $\sim 1/8100$ for a Si target). Using $p > 8$ GeV/c for the 3 muons and the rough efficiency estimates given above, one obtains an estimate of 12200 $3\,\mu\pi^+\pi^- X$ events/year (with $L = 10^{32}$ cm^{-2} s^{-1}).

In the framework of the present discussion we made some suggestions concerning the qualities of a forward spectrometer. We considered the characteristics of pixel vertex detectors, CRIDs, and muon detectors. Triggering methods in a forward spectrometer were also discussed.

We have also mentioned advantages and disadvantages of interactions with fixed targets (point 3). For an external target, a beam intensity of at least 10^8 p/s would be necessary in order to search for CP violation in B decay. About $\sim 10^{10}$ $pp \rightarrow b\bar{b}X$ events would then be expected per year ($\sim$ 10 times less than in the central collider case). With a gas-jet target, there is no difficulty in obtaining $b\bar{b}X$ events, as the intensity of the internal SSC beam is large (4.4×10^{17} p/s). However, multiple interactions per bunch crossing will complicate the analysis, since the gas-jet target appears as a point-source. This might, for instance, complicate the identification of the correct muon tagging. A decrease in the luminosity could be obtained by decreasing the gas-jet density. Assuming that the ratio of two interactions per bunch crossing to one is 0.025 for minimum bias events, one produces 10^9 $b\bar{b}X$ events per year ($\sim$ 10 times less than the external target case).

In summary, the SSC provides an excellent opportunity for studying B-physics. Interest has already been shown by a large number of physicists. As discussed above, cost effective detectors may be designed to study the B mesons produced in pp collisions. The present studies must be extended to optimize the designs of the detectors.

References

1. K. J. Foley et al., Proc. Workshop on Experiments, Detectors, and Experimental Areas for the Supercollider, Berkeley, July 7–17 (1987);
   M. M. Block and R. N. Cahn, Phys. Lett. 188B, 143 (1987); M. M. Block, F. Halzen and B. Margolis, NUHEP Report No. 171, McGill Preprint 91–23, July 1991;
   E. L. Berger and R. Meng, Heavy Quark Cross Section at Hadron Collider Energies, Argonne report, ANL–HEP–PR–91–11 (1991).
2. I. I. Bigi and A. I. Sanda, Nucl. Phys. B193, 85 (1981).
3. I. I. Bigi, UND–HEP–91–BIG02 Report (1991), to be published in Proc. "Les Rencontres de Physique de la Vallée d'Aoste," La Thuile, Italy, March 1991.
4. A. Fridman and A. Snyder, Proc. Large Hadron Collider Workshop, Aachen, 4-9 October 1990, Vol.II, p. 218, CERN 90–10 (1990).
5. A. Fridman, CERN–PPE/91–113 Report (1991) and Proc. 3th Topical Seminar on Heavy Flavor (Nucl. Phys.), San Miniato, 17–21 June 1991.
6. M. Chaichian and A. Fridman, Measurement Possibilities of CP Violation for B Decays in pp collisions, CERN–TH.6068/91 (1991);
   A. Fridman, CERN–EP/90–87, CERN Report (1990).
7. T. Sjöstrand, private communications.

8. PYTHIA, H-U. Bengtsson and T. Sjöstrand, Comp. Phys. Commun. 46, 43 (1987).
9. ISAJET, F. E. Paige and S. D. Protopopescu, ISAJET 6:21.
10. I. I. Bigi and A. I. Sanda, Nucl. Phys. B281, 41 (1987).
11. Expression of Interest, Solenoidal Detector Collaboration, May 24, 1990.
12. An expression of Interest to Construct a Major SSC Detector, July 8, 1991.
13. M. Cannalire and A. Fridman, Dilution Effects for CP Violation Measurement in B decays, SSCL–566, SSC Report (1992).
14. The Physics Program of a High-Luminosity Assymmetric B Factory at SLAC, SLAC–353 Report (1989);
Natalie Roe, LBL Reports and D0 notes, 1022 (1990) and 1122 (1991).
15. A. Ali, DESY 91–080 Report (1991);
M. J. Savage, RU–91–22 Report (1991).
16. A. Fridman and A. Snyder, Importance of the $B_s^0 \to \mu^+\mu^-$ Branching Fraction, SLAC–PUB–5644 (1991).
17. Expression of Interest in a Super Fixed Target Beauty Facility at the SSC, May 25, 1990.
18. PAPAGENO program written by I. Hinshliffe (LBL).
19. Expression of Interest for Bottom Collider Detector at the SSC, May 25, 1990.
20. R&D for Collider Beauty Physics at the LHC, CERN/DRDC 91–18 Report, 22 March 1991.
21. Radiation Levels in the SSC Interaction Regions, SSC–SR–1033 Report (1988).
22. See for instance, S.Fredrickson et al., Phys. Rep. 144, 187 (1987), and quoted references.
23. F. Fumuro et al., Nucl. Phys. B152, 376 (1979).
24. S. J. Brodsky and P. Hoyer, Phys. Rev. Lett. 63, 1566 (1989).
25. A. Fridman and A. Penzo, CERN–PPE/9158 Report (1991), and Proc. 3^{rd} Topical Seminar on Heavy Flavor (Nucl. Phys.), San Miniato, 17–21 June 1991, and quoted references.
26. D. M. Alde et al., Phys. Rev. Lett. 66, 2285 (1991).
27. See for instance, M. J. Tannenbaum, Int. Jour. of Mod. Phys. A, Vol. 4, No. 14, 3377 (1989), and quoted references.
28. T. Kanki et al., Progress of Theoretical Phys., Supplement 97B, 1 (1989).
29. Proc. "B-Physics with SSC Experiments," SSC, January 21–22, 1992, Eds., A. Fridman and J. Siegrist.
30. Rosen, Internal Target Beauty Physics at the SSC Introduction, SSC–E0I0013.
31. A Study of CP Violation in B-Meson Decays using a gas-jet at LHC, January 1992.

Appendix A

Accelerators Issues

Several questions related to the accelerator design and performance for studying B-physics have been considered. Some of these questions will be discussed here.

A1 - Collider experiments

A1.1 - The luminosity

In the first phase of collider operation, a luminosity of $L = 10^{33}$ cm^{-2} s^{-1} is forseen. A static change of L can easily be accomplished by increasing β^* from the design medium range (10 m) to a large value (100 m), corresponding to a luminosity of 10^{32} cm^{-2} s^{-1}. Dynamically, i.e., during the run, L could be decreased by enlarging the beams in the transverse dimension ($\sigma_{x,y} = 5$ μm).

A1.2 - The bunch spacing

It might be advantageous to have more time between the bunch crossings (now 16.7 ns). This allows detector signals time to settle and to have the system cleared before a new event occurs. Normally, a change in the bunch spacing would be effected in the injector system, affecting all the other interaction regions (decreasing an effective luminosity). Another way of increasing the bunch spacing in one experiment (to 170 ns, for instance) while not affecting others, is to move electrostatically nine out of ten bunches in the transverse direction. A deviation of 2.5 μm would shift the mean of the transverse beam position by a total of 10 $\sigma(x, y)$. This leads to a decrease of L by a factor of 10^5 for the nine out-of-focus bunches. A detailed study is under way to determine the feasibility of this method. In any case, the main difficulty is that the 20 TeV beam is very rigid, and one must collect the moved bunches at the end of the drift region.

A1.3 - The dimensions of the intersection region (IR)

The drift length in the interaction region will be $\pm$120 m for medium luminosity IRs. This dimension is large enough to avoid restrictions for the overall detector layout.

A2 - The fixed target

An external 2 TeV/c beam is planned for 1996, near the high energy booster (HEB) at the West Campus. Due to the overall layout of the collider abort lines, the utilization of 20 TeV/c beams will not be possible in this area. At the East Campus, however, the possibility of having fixed target facilities with a beam of 20 TeV/c will be investigated.

A3 - The Gas-Jet

It is believed that there will be no degradation of the collider beams during a gas-jet experiment. One must keep in mind that the two colliding beams are separated by 80 cm in the region where a gas-jet experiment would be carried out.

Reference

1. Site-Specific Conceptual Design, SSCL–512–1056 (1990).

Appendix B

Dilution Effects

The difficulties of comparing the number of l^+fX (N_+) and l^-fX (N_-) events in a given experiment in order to search for CP violation in $B^0, \bar{B}^0 \to f$ have been discussed[4] (the quoted references are those given in the text). Here f is assumed to be a self conjugate state ($f = \bar{f}$) while the tagging of the associated beauty particle is given by the charge of the lepton ($l^\pm$) in its semileptonic decay ($B \to l^+X$, $\bar{B} \to l^-X$). For simplicity we will consider semileptonic decays into muons.

A CP violation effect in the decay will be observed if

$$A = \frac{N_+ - N_-}{N_+ + N_-} \neq 0 .$$

The number of events $N = N_+ + N_-$ necessary to observe a given asymmetry A with $s = A/\Delta A$ standard deviations is then given by

$$N = s^2 \left[\frac{1}{A^2} - 1\right] .$$

Practically, the measured A value is affected by a dilution effect due to the mistagging of the muon.[13,14] Here we use a somewhat different approach to estimate the dilution for hadron-hadron interactions at large center-of-mass energy[13] (for instance, $\sqrt{s} > 0.1$ TeV).

The muon mistagging can be due to:

(1) the mixing of B_d^0 or B_s^0 ($\bar{B}_d^0$ or $\bar{B}_s^0$) before decaying into muons,

(2) the cascade $b \to c \to \mu$ ($\bar{b} \to \bar{c} \to \mu$) where the μ has the opposite charge of the $b \to \mu$ ($\bar{b} \to \mu$) decay,

(3) the μs coming from other decaying particles ($K, \pi \ldots$),

(4) the punchthrough in the detector (particles identified wrongly as muons).

The first case leads to the prediction given by[13]:

$$A = \left[\frac{nx_d}{1+x_d^2}\,(p_\pm + p_\Lambda) + \frac{n(x_d + x_s)}{(1+x_s^2)(1+x_d^2)}\,p_s + \frac{nx_d}{(1+x_d^2)^2}\,p_d\right] .$$

Here $n \equiv \sin 2\phi$ is the CP violation parameter. The $p_\pm$, p_d, p_s, and p_Λ quantities are the production rates of the $B^\pm$, B_d^0, B_s^0, and Λ, respectively, and taken as:

$$p_\pm : p_d : p_s : p_\Lambda = 0.38 : 0.38 : 0.14 : 0.10 .$$

The mixing of the $B^0_{d,s}$ is given by the $x_{d,s}$ parameters related to the mixing by:

$$\alpha_{d,s} \equiv \frac{N(B^0_{d,s} \to \bar{B}^0_{d,s})}{N(B^0_{d,s} \to B^0_{d,s}) + N(B^0_{d,s} \to \bar{B}^0_{d,s})} = \frac{1}{2}\,\frac{x^2_{d,s}}{1+x^2_{d,s}}\ ,$$

$$\beta_{d,s} \equiv \frac{N(B^0_{d,s} \to B^0_{d,s})}{N(B^0_{d,s} \to B^0_{d,s}) + N(B^0_{d,s} \to \bar{B}^0_{d,s})} = 1 - \alpha_{d,s}\ ,$$

(as above, N denotes the number of events). Based on the actual experimental data one has $\alpha_d \simeq 0.16$. For the B^0_s mixing one usually uses $\alpha_s \simeq 0.5$, as one expects that $x_s \geq 8$. Note that by tagging only charged particles, one will have an asymmetry parameter $A_\pm = n x_d/(1+x^2_d)$, while in the general case

$$A = A_\pm \times 0.77 = \sin 2\phi \times 0.35\ ,$$

using $x_s = 8$ and the production rates ratios given above.

Let us now discuss the effects due to the mistagging of the muons (cases 2 to 4). In practice one will measure an asymmetry parameter A_m containing also the effects due to the mistagging of the muons. Assuming that the true (wrong) number of events is represented by $N^c_\pm$ ($N^w_\pm$), one has

$$A_m = \frac{N^c_+ + N^w_+ - N^c_- - N^w_-}{N_t}\ ,$$

where N_t represents the total number of (true and wrong) tagged events. The real A value and the fraction of wrong tagging (w) are here defined by

$$A = \frac{N^c_+ - N^c_-}{N^c_+ + N^c_-} = \frac{N^w_- - N^w_+}{N^w_+ + N^w_-}\ ,$$

$$w = \frac{N^w_+ + N^w_-}{N_t} = 1 - \frac{N^c_+ + N^c_-}{N_t}\ ,$$

yielding thus, $A_m = A(1-2\,w)$. For an estimate of w we do not use here cases 3 and 4, which depend on the detector of the experiment. Using the branching ratios of the beauty and charmed hadrons given in Ref. 13, one obtains from the cascade decays, $w \simeq 0.31$. This corresponds to

$$A_m \simeq A_\pm \times 0.77 \times (1-0.62) = \sin 2\phi \times 0.13\ .$$

With these approximations and the number of events estimated in the central region (Section 3.1), the minimum value of $|\sin 2\phi|$ that could be observed with three standard deviations after two years of running would be $|\sin 2\phi|_{\rm min} \simeq 0.31$. For the events appearing in the forward cone, one has $|\sin 2\phi|_{\rm min} \simeq 0.15$ (two years of running).

In the present discussion the cascade decay ($b \rightarrow c \rightarrow \mu$) appears to be important. Kinematical cuts could decrease this effect but will also decrease the number of events with B_d^0 decays. Further investigations must be made for a given experiment, as cuts will depend on the detector properties. In that case one has also to estimate the mistagging effect due to muons coming from K and π decay and to the punchthrough effect.

Appendix C

Pixel Detectors

Silicon PIN diode array hybrids have been discussed in the literature of the SSC for a number of years.[1,2] These devices are ideal candidates for vertex detectors which can reconstruct secondary vertices close to the primary interaction point. They are radiation hard, have fast response time, and have fine multiple particle resolution. Pixel arrays provide three-dimensional coordinate information with fine spatial resolution both along the beam direction and in the transverse direction. This high resolution information allows fast algorithms for track identification and pattern matching in a low-occupancy environment. This allows a reduction in the number of detector elements, when compared to microstrip detectors, thereby reducing detector mass. They are intrinsically radiation resistant because detector leakage current and its associated noise is partitioned among a very large number of pixel elements. The very high signal-to-noise ratio, at least 100:1, provides both robust performance in the SSC environment and allows room temperature operation.

The Generic Detector Development R&D program funded by the SSC Laboratory saw the first implementation of these hybrid arrays in the detection of high energy particles, although they had been in use for many years for infra red and x-ray detection. The Pixel Detector Collaboration[3,4] was established to develop a vertex tracking capability utilizing improved versions of these hybrids, specifically for experiments at the SSC. Progress reports on these developments for the years 1990 and 1991 have been submitted to the SSC Laboratory.

A brief summary of the development effort is described in this appendix, and in the references and progress reports mentioned:

- A prototype of a single pixel cell of a proposed array has been designed and fabricated in a nonradiation-hard CMOS technology, and has successfully demonstrated a noise level of less than 200 electrons. The pixel dimensions are 50 μm $\times$ 150 μm.
- An array of these pixels which is 32 $\times$ 64 has demonstrated the concept of time stamping, i.e., correlating the time of arrival of a particular hit with the pulse height and address of the hit.
- A radiation-hard version of the SSC pixel cell has been designed and fabricated in an SOS/CMOS process. It is presently being tested.
- A more robust, radiation hard pixel cell design with autonomous operational characteristics has been designed and fabricated. Preliminary tests generally meet performance goals.

- Ideas for low-mass mounting and cooling of the vertex detector elements based on low-mass ceramic foams have been developed.

During the next few years, a vigorous research effort in this state-of-the-art vertex detector technology will be continuing. The short term goals of this effort would be to:

- complete the process of selecting a radiation hard technology so that a 10 MRad hard array can be demonstrated,
- produce a large array with a simple peripheral architecture based on our existing 32×64 array. This array would be about 1 cm^2 in area, and would have pixels which are 50 μm by 150 μm.
- continue the radiation testing of rad-hard arrays, and the beam testing of all new arrays as they become available

References

1. J. G. Jernigan, J. Arens, G. Kramer, T. Collins, J. Herring, S. L. Shapiro, and C. Wilburn, "Performance Measurements of Hybrid PIN Diode Arrays," Proc. 1990 Int. Industrial Sym. on the SSC, Miami Beach, Florida; SLAC–PUB–5211.
2. S. Shapiro, J. G. Jernigan, J. Arens, G. Kramer, T. Collins, S. Worley, C. Wilburn, P. Skubic, "Performance Measurements of Hybrid PIN Diode Arrays," Proc. Sym. on Detector Research and Development for the Superconducting Supercollider, Fort Worth, Texas, 1990, p. 139; SLAC–PUB–5357.
3. O. Barkan, E. Atlas, W. L. Marking, S. Worley, G. Y. Yacoub, G. Kramer, J. Arens, J. G. Jernigan, S. L. Shapiro, D. Nygren, and H. Spieler, "Development of a Customized SSC Pixel Detector Readout for Vertex Tracking," Proc. Sym. on Detector Research and Development for the Superconducting Supercollider, Fort Worth, Texas, 1990, p. 142; SLAC–PUB–5358.
4. J. Arens, J. G. Jernigan, S. Mani, D. Pellett, G. Atlas, S. Augustine, O. Barkan, T. Collins, G. Kramer, C. Pfeiffer, D. Wolfe, S. Worley, G. Yacoub, S. Holland, D. Nygren, H. Spieler, M. Wright, P. Gutierrez, P. Skubic, S. Shapiro, P. Mockett, V. Cook, "Progress Report of the Collaboration for Development of Pixel Vertex Detector Technology," Submitted to the SSC Laboratory on September 15, 1991.

Appendix D

Preliminary Design of a Vertex Detector

D1 - Introduction

A number of proposals have been advanced for the study of B physics in pp interactions at the SSC. In this section, a preliminary design for a vertex detector for use in a forward spectrometer is presented. A forward spectrometer for the detection of Bs is an attractive idea for many reasons:

- The forward direction contains the lion's share of the Bs produced,
- In the forward direction there is a high probability that both the B and the $\bar{B}$ will be produced in the same angular region,
- The forward boost may make the detection of leptons (muons) easier, and potentially provide a lepton trigger for the Bs,
- The small angular region of interest should translate to a more affordable experiment.

D2 - The preliminary design specifications

- The vertex coverage is to be in the angular region from 1–10° to the beam line.
- The vertex detector is to be in a field-free region.
- For the purpose of this exercise, a minimum of four detectors (disks) are placed along the trajectory of each particle, each giving a three-dimensional space point. When more details are known about the fill factor of each detector array, and the packing fraction of arrays onto each disk, a Monte Carlo calculation will refine this number.
- Cost is a consideration. Wherever possible, modularity of design is to be attempted.
- To reduce multiple scattering, mounting and cooling techniques should employ state-of-the-art, low-mass materials. Ceramic foam has been chosen in this example.

Figure D.1 is a schematic of the vertex detector. It covers the angular cone of 1–10° to the beam axis. It employs 13 disks spaced along the beam line, and three 10 cm-long cylinders about the central region having radii of 3, 4, and 5 cm. All of the disks have a 2.5 cm radius cut from the center. Eight of the disks have a 10 cm outer radius while the remaining five disks have an outer radius of 8, 8, 6, 6, and

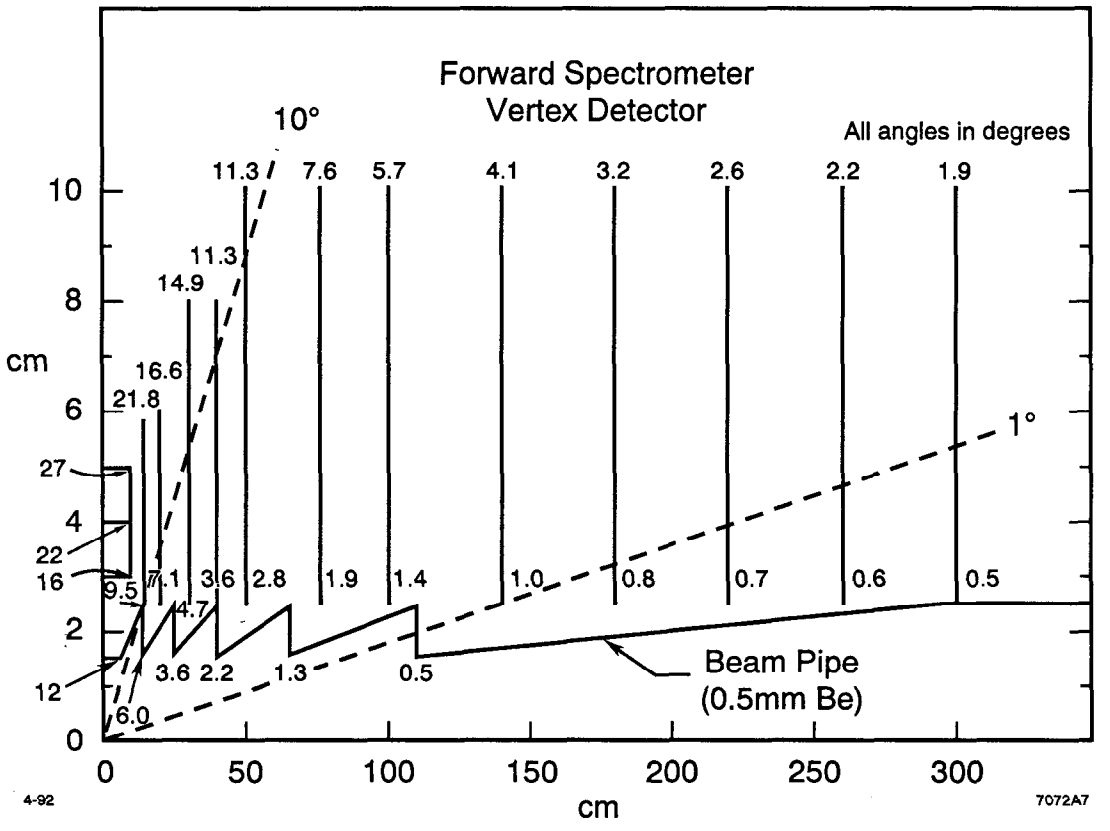

Figure D.1. A schematic of the vertex detector for the forward spectrometer comprised of 13 discs and 3 small cylinders. The geometry has been chosen to insure at least 4 hits per track in the forward $1 < \Theta < 10°$ cone. An illustration of a thin beam pipe is also presented.

5 cm respectively. The area coverage of these thirteen disks is about 3,700 cm^2. It is proposed that we mount pixel detectors whose area is approximately 1 cm^2 on these disks. The pixel arrays are those described in the preceding appendix. The pixel size is 50 $\mu m \times 150$ μm. As research progresses, detectors having a small square pixel size (< 50 μm on a side) may become available.

The inner dimension, 2.5 cm, has been chosen conservatively. At a luminosity of 10^{33} cm^{-2} s^{-1} there would be a radiation dose rate of about 10 MRad/year at a radius of 2 cm. This figure does not include "loopers" since this is a field-free region. However, this experiment is envisioned to run at a luminosity of 10^{32} cm^{-2} s^{-1}. Thus, at a radius of 2.5 cm, the dosage would be less than 1 MRad/year. If the arrays are radiation hardened to 10 MRad, this figure would appear to be conservative.

As for neutron damage, the forward region does not have a calorimeter surrounding it, and there is no issue of "albedo" neutrons. Nevertheless, the number

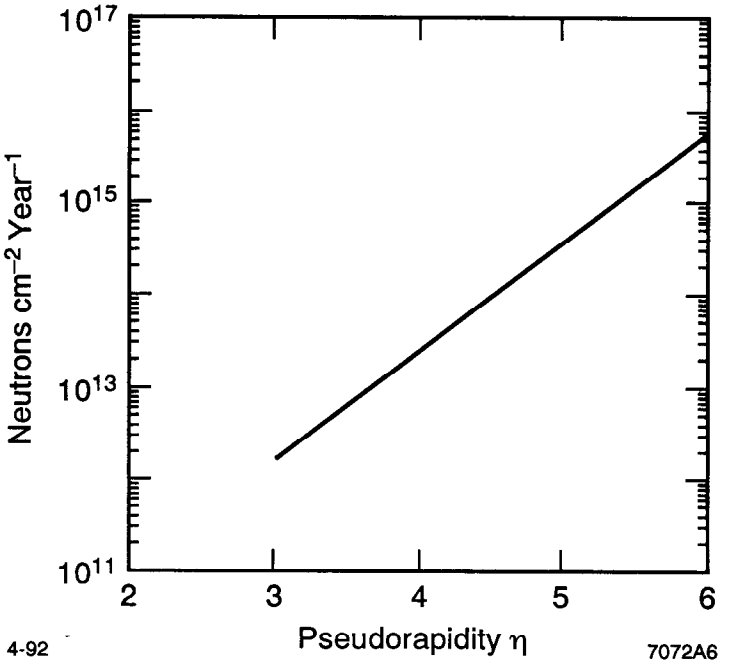

Figure D.2. Neutron flux as a function of pseudorapidity at a luminosity of $L = 10^{33}$ cm^{-2} s^{-1}.

of neutrons produced in the forward region is high. Figure D.2 is a curve of neutron flux as a function of pseudorapidity (η). At design luminosity, the number of neutrons per cm^2 per year is[1] 4×10^{14} (at $\eta = 5$). At our luminosity this number is down by an order of magnitude. Furthermore, the bulk of the detector is at $\eta < 5$. At these levels the PIN diodes will be effected. They will tend to undergo type-inversion. However, recent studies seem to indicate that there is life after type inversion.[2] With this in mind, it is wise to develop a mounting technique which allows the inner radius of the disk to be replaced every so often with new arrays. A brief calculation will demonstrate that this will be necessary to only a few of the arrays, and does not represent a large expense.

D3 - A few rudimentary resolution numbers

Precise vertex resolution is essential for doing B physics at the SSC. In the absence of multiple Coulomb scattering, the spatial resolution of a track at a vertex is:

$$d = \sigma\sqrt{n}\ S/L\ ,$$

where σ is the intrinsic spatial resolution of the detector, n is the number of planes, S is the distance from the vertex to the first plane, and L is the distance from the

first plane to the last crossed by the track. For the geometry shown in Figure D.1, a track will cross four or five detectors. The arrays will be rotated so that on average two of the arrays will give resolution consistent with the small dimension of the pixel (50 μm) and two of them will give resolution typical of the larger dimension (150 μm). The resulting spatial resolution per track at the vertex is less than 5 μm.

In the forward direction, the largest contribution to the error in determining the vertex position will, of course, come from multiple Coulomb scattering. This contribution, in a plane, is:

$$d\ (\mu\text{m}) = 8.0\ R_t\ (\text{cm})/p_T\ (\text{GeV/c})\ ,$$

where R_t is the perpendicular distance of the track from the beam line. This error pertains to the amount of material found in a 250 μm thick silicon hybrid detector. This detector will have PIN diodes 200 μm thick, and readout electronics back-thinned to 50 μm. The detector hybrid is mounted on a boron carbide (B_4C) foam support which has been foamed to 3% of its nominal density (X_0 = 600 cm). Since Beauty decay particles have transverse momentum (p_T) of between 1 and 2 GeV/c, this source of error can be on the order of 24 μm for a track traversing a single array and having a p_T of 1 GeV/c. For tracks traversing all four arrays, at approximately equal spacing, the vertex resolution will be only slightly improved, since the error from the latter disks that will be intercepted at larger R_t will be larger.

To do B Physics, it is essential that "d" be much less than $c\tau$ for Beauty (about 300 μm). Thus, the disks must have their inner radius as close to the beam line as possible. In this design, R_{min} has been chosen to be 2.5 cm. More detailed Monte Carlo calculations on beam line details may allow for a smaller inner radius as radiation problems become better understood. As R_{min} decreases, vertex resolution gains linearly.

A plot of vertex resolution versus the angle of the track is found in Fig. D.3. The horizontal axis is measured in degrees. For a track having a total momentum P of 13.6 GeV/c, the axis can also be labelled in units of transverse momentum p_T as shown.

D4 - The beam pipe

The beam pipe design plays an important role in minimizing multiple Coulomb scattering. The conical design, shown in Fig. D.1, has been selected for ease in analysis. Many beam pipe configurations are possible, and the optimum is uncertain at this time.

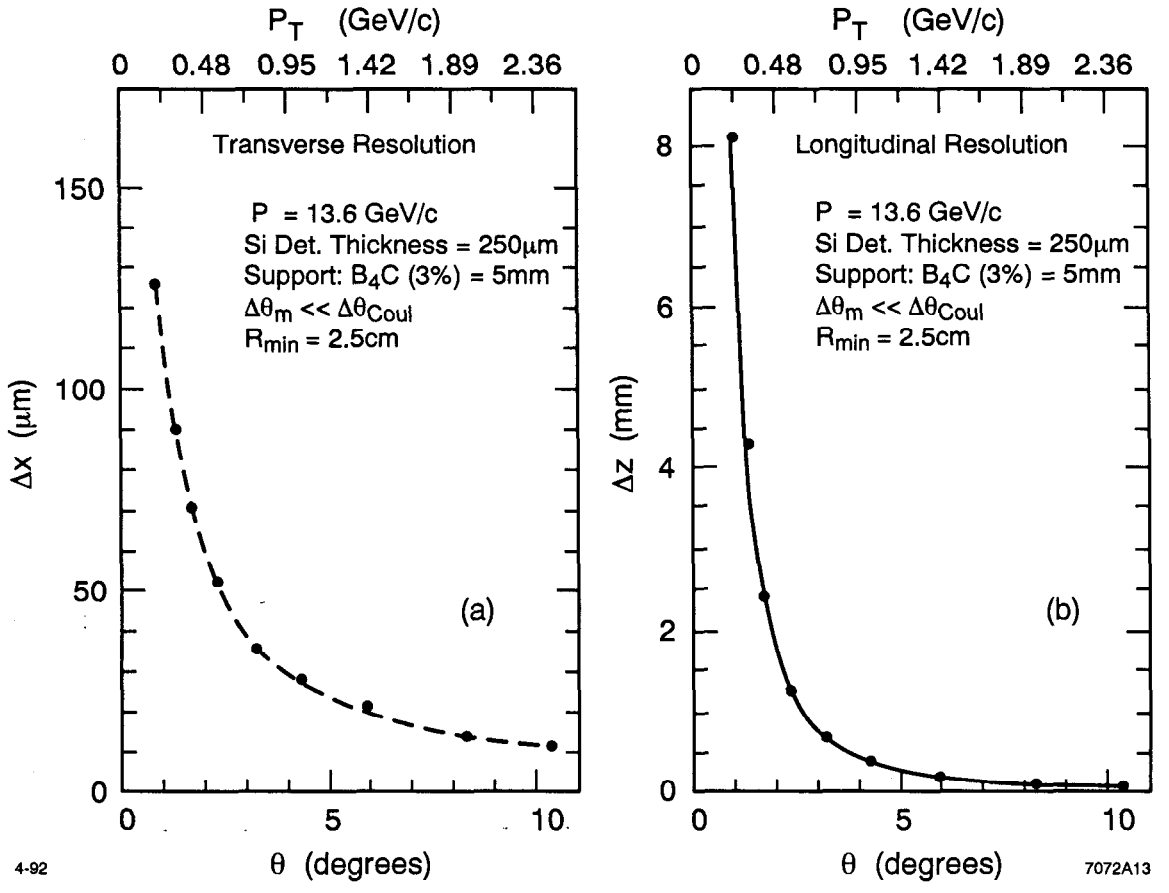

Figure D.3. Plots of transverse and longitudinal resolutions for 13.6 GeV momentum tracks. The p_T values corresponding to the 13.6 GeV track are shown on the top axis. Note that B decay tracks have an average transverse momentum of ~ 2 GeV/c.

In this design, a 0.5 mm thick beryllium tube with an inner radius of 1.5 cm begins to taper to a radius of 2.5 cm. The taper begins at $z = 7$ cm and reaches a 2.5 cm radius at $z = 14$ cm. At this z position, it steps back to 1.5 cm in radius and begins another taper back to a 2.5 cm radius, which it reaches at $z = 24$ cm. This process is repeated, producing additional steps at $z = 40$, 66 and 110 cm. Thus, all of the particles of interest pass through a vertical disk of 0.5 mm thick beryllium, except for those at exactly 6°, 3.6°, 2.2°, and 1.3°.

If this were a single, 0.5 mm thick tube of beryllium having a 1.5 cm radius, it would withstand an outside pressure of about 26 atmospheres. As it is tapered, and is not a perfect tube, additional mechanical calculations must be done before making the walls thinner. At this thickness, and using the above design, the error in the

determination of the decay vertex is increased by about 30 μm for a particle that crosses the beryllium at an R_t of 2 cm and has a p_T of 1 GeV/c.

Choosing the inner radius of the beam pipe to be 1.5 cm, allows for an aperture-filling beam during injection, and guarantees that any beam scraping will occur elsewhere in the machine.

This vertex detector design highlights the various sources of error and attempts to minimize them. The primary source of uncertainty is not measurement error, but is multiple Coulomb scattering in the beam pipe and the detector disks. Measurement error is kept small by using small pixels and ensuring that the extrapolation distance is always less than or equal to the distance over which we make the measurement. As for multiple scattering, one must await detailed calculations and simulations before proposing the use of thinner detectors, supports, and/or beam pipe. The use of pixel detectors does , however, result in the minimization of the overall mass of the vertex detector, and thus the multiple scattering error is minimized as well.

References

1. D. Groom, "Radiation Levels in SSC Detectors," Proc. Summer Study on High Energy Physics in the 1990s (World Scientific, 1988) p. 711.
2. D. Pitzl et al., "Type Inversion in Silicon Detectors," SCIPP 91/05 (1991); F. Lemeilleur et al., "Neutron-Induced Radiation Damage in Silicon Detector," CERN-ECP 91-21 (1991).

Appendix E

Cherenkov Ring Imaging at the SSC

E1 - General comments

Cherenkov ring imaging detectors (CRIDs) were first proposed by Ypsilantis and Sequinot[1] to aid in the identification of particle masses. Reference 2 shows an example of such an application in an SSC experiment.

To identify pions and kaons in B physics experiments, one needs Fast Cherenkov Ring Imaging (Fast CRID). The momentum distribution of the B decay particles in the region $1 < \Theta < 10°$ is presented in Fig. 4.4. Most of these particles have a momentum smaller than 100 GeV/c.

The maximum momentum $P_{\max}$ that allows two particles having masses m_1 and m_2 to be separated by n_σ standard deviations is given by the following approximate relation:

$$P_{\max} = \sqrt{\frac{LN_0(m_1^2 - m_2^2)}{2(\Delta\Theta_c/\Theta_c)\, n_\sigma\sqrt{N}}} \quad ,$$

where $N = N_0 L \sin^2\Theta_c$ and $\Theta_c = \cos^{-1}(1/\beta n)$. Here n is the index of refraction of the medium, L is the length of the detector and N is the number of photoelectrons on the Cherenkov ring. N_0 is a "figure of merit" related to the detector design and $\Delta\Theta_c/\Theta_c$ is the resolution of the Cherenkov angle. N can be calculated given N_0, L and n. The above equation is valid only for large γ and for the case that the detector pixel spatial resolution is of the order of 1 mm or less.

In the following estimates, a number of very conservative assumptions have been made, rather than employing "best-ever figures." Furthermore, it should be emphasized that a detailed Monte Carlo calculation must be made to demonstrate the final effectiveness of CRIDs in particular physics channels. The Cherenkov angle resolution is typically dominated by chromatic errors, the change of the refractive index n with wavelength. Typically, one obtains $\Delta\Theta_c/\Theta_c = 3 \times 10^{-3}$ for gases such as helium, CF_4, C_2F_6 and C_4F_{10}. However, the high multiplicity environment at the SSC may enlarge $\Delta\Theta_c/\Theta_c$, due to extra hits on a ring caused by overlapping rings and high occupancy. We, therefore, take the more pessimistic number $\Delta\Theta_c/\Theta_c = 10^{-2}$. In the calculation of P_{max}, it is traditional to choose $n_\sigma = 3$. Again, due to the confusion and high multiplicity at the SSC, all momentum estimates use $n_\sigma = 4$.

In this embryonic design, a CRID with a gaseous C_2F_6 radiator operating at normal temperature and pressure is proposed. The counter uses spherical mirrors at its downstream end to focus the UV photons back onto a photon detector at the upstream end of the counter. The photon detector will be placed as far away from the

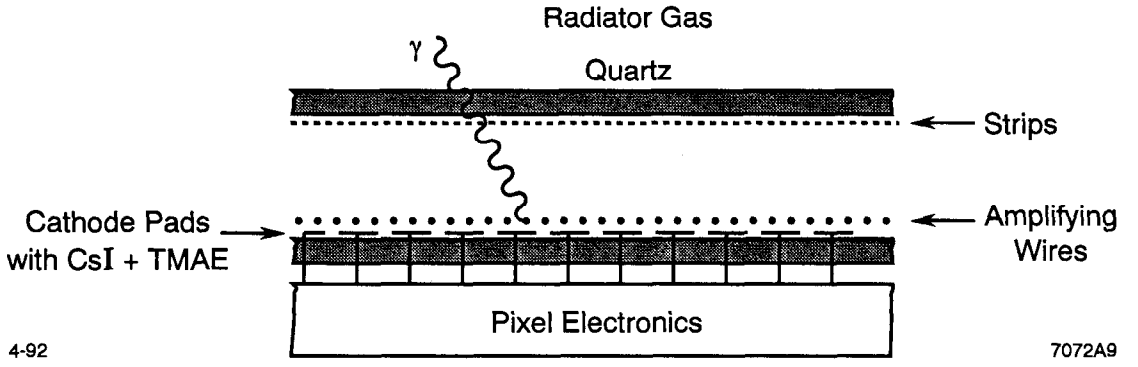

Figure E.1. A single electron counter based on wire amplification.

beam line as possible to avoid radiation damage. The length of the counter L has been chosen to achieve an N of about 30 photoelectrons. For the C_2F_6 radiator this means a length of about 4 m, assuming a modest N_0 of about 50 cm^{-1}. Again, $N_0 = 50$ cm^{-1} is a rather conservative figure; the actual calculations for the embryonic design show that it should be possible to achieve more than 75 cm^{-1}. An initial configuration of the spectrometer should assume one such CRID placed downstream of the dipole.

E2 - Single electron detection considerations

The photon detector must have a high efficiency for conversion of the UV photons. It must be fast, it must survive very high doses of charged radiation, and it must be compatible with a very long length radiator that causes a loss of photons due to gas absorption. This last requirement eliminates the possibility of using TEA as a possible photosensitive gas.

Presently there is very active research studying the various types of gaseous and solid photocathodes.[2–6] In particular, the work using CsI photocathodes with adsorbed TMAE on the surface appears to be promising. The CsI+TMAE photocathodes are found to have a quantum efficiency higher than TMAE-loaded gaseous photocathodes, namely $> 35\%$ in a photon energy window between 6 and 7 eV (Ref. 4). The photocathode is deposited on the cathode surface, which has been divided into a pad structure. An example of a gaseous photocathode would be 80% CF_4+20% iC_4H_{10}+TMAE (60°C, Ref. 7). Electrons liberated from the photocathode can be amplified either on the wires[2] or in a parallel plate structure (PPAC).[5,6]

We have chosen the more conservative design, that of an amplifying structure described in Fig. E.1. It has a quartz window on which are deposited cathode strips to define voltages. Amplification is done on anode wires placed 0.5 mm away from the

cathode pads to get sufficient coupling efficiency.[2] For single electron detection, wire amplification is preferred, compared to PPAC, because it is less prone to sparking in extremely noisy environments.[7] The Cherenkov photons are converted to electrons using a solid photocathode made of a CsI+TMAE layer deposited on the cathode pads. The induced signal on the pads is then used to localize the UV photon. The detector gas is either CH_4+iC_4H_{10} or 80% CF_4+20% iC_4H_{10} mixture to provide good quenching.

One should stress that the solid photocathodes are probably more fragile when compared to gaseous photocathodes, such as TMAE, TEA, etc. More studies of aging and of sensitivity to other kinds of damage must be completed before an engineering proposal can be made. The detectors must operate at as low a wire gain as possible to achieve their maximum usable life.

The detector can be read out by pixel electronics[8] or VLSI electronics, as described by Arnold et al.[2] In the former case, in order to match the pixel dimension to the detector pad structure, a special adapter must be developed or a modified readout produced. It is important to note that the use of a pixel array enables the time stamping of the Cherenkov ring. Even if the rings overlap those from noninteresting tracks, the rings from the noninteresting tracks can be eliminated by use of the time information.

E3 - Separation

P_{max} is the momentum that allows $4\,\sigma$ particle separation. P_{min} is defined to be the momentum that results in half the number of photoelectrons in a typical ring. Using an N_0 of 50 cm^{-1} and a length $L = 400$ cm, one can achieve the results shown in Tables E.1 and E.2 for the Cherenkov counter.

Table E1

	π/K	e/π	e/μ
P_{max} (GeV/c)	95	29	19

Table E2

	π	K	μ	e
Threshold	3.5	12.0	2.6	0.0125
P_{min} (GeV/c)	4.9	17	13.7	

References

1. T. Ypsilantis and J. Seguinot, Nucl. Instrum. Meth. 142, 377 (1977).
2. T. Ypsilantis, "RICH/CRID for future hadron collider experiments," presented at the 1988 Snowmass Conf., Snowmass, Colorado.
   R. Arnold, Y. Giomataris, J. L. Guyonnet, A. Racz, J. Sequinot, and T. Ypsilantis, CERN-LAA/PI/91-014, 1991.
3. A. Breskin et al., Instr. in Astronomy, 1235, 896 (1990).
4. J. Sequinot et al., CERN-EP/90-88, 1990.
5. D. Anderson et al., FERMILAB-PUB-90/182, 1990, Nucl. Instrum. Meth. A309, 377 (1991) and Fermilab Tech. Note TM-1753, 1991.
6. P. Fonte, V. Peskov, and F. Sauli, Nucl. Instrum. Meth. A310, 140 (1991).
7. J. Va'vra, SLAC-PUB-5793 (1992).
8. J. G. Jernigan et al., "Performance Measurements of Hybrid PIN Diode Arrays," Proc. 1990 Int. Industrial Sym. on the SSC, Miami Beach, Florida, 1990; SLAC-PUB-5211;
   S. Shapiro et al., "Performance Measurements of Hybrid PIN Diode Arrays," Proc. Sym. on Detector Research and Development for the Superconducting Supercollider, Fort Worth, Texas, 1990; SLAC-PUB-5357;
   O. Barkan et al., "Development of a Customized SSC Pixel Detector Readout for Vertex Tracking," Proc. Sym. on Detector Research and Development for the Superconducting Supercollider, Fort Worth, Texas, 1990; SLAC-PUB-5358.

Appendix F

Triggering Considerations

F1 - Introduction

Various triggering signatures on bottom production are considered for the particular case of correlated $B\bar{B}$ production in the forward direction. Recommendations are made for a possible configuration of a trigger that is applicable to the generic design of a forward spectrometer. Lack of a detailed Monte Carlo simulation renders some aspects of the discussions qualitative, but an attempt is made to quantify the rates at the level of orders of magnitude.

Even though the cross section for $B\bar{B}$ production is by some estimates as high as 1/300 of the total cross section at the SSC, triggering requirements are quite strict because the highest possible rate is desired in order to fully exploit the high luminosity. For studying CP violation, large statistics are required in a few, specific decay channels of the B meson that typically have very small branching ratios. Efficient tagging of the partner B meson flavor puts further constraints on the decay channels. Even though the ultimate limit to the rate of triggered events may well come from the detector components, an effort has been made to fully maximize the rate capabilities of the trigger. A "loose" trigger, desirable from the standpoint of simplicity, is not likely to provide the necessary rejection of backgrounds so that the data acquisition rate can be matched. Dilution effects further raise the level of statistics required, and also demand suppression of backgrounds to the tagging channel. This also implies that the trigger should not be too biased, in order to allow for enough statistics to study the topology of background events, and implement effective off-line cuts. The problem of triggering is approached with the additional constraint that the detector geometry is sensitive only to a correlated production of the $B\bar{B}$ pairs in the forward direction.

A conservative approach for triggering on B production would be to consider a variety of signatures, and to implement a strategy that exploits these signatures in various logical combinations and levels. In the following, various options and their respective advantages and drawbacks are discussed.

F1.1 - Semileptonic decay channel

This is a conventional method for triggering on heavy quark production, because of the relatively high semileptonic branching ratios. Tagging one of the pairs of heavy quarks for its flavor quantum number is an essential part of the physics analysis for studying CP violation. The leptons prove convenient for this purpose, as well. However, a threshold cut on the p_T of the lepton is usually required, which lowers the

efficiency of the trigger. In addition, the electron channel suffers from an enormous background that is the result of conversions of photons from pion decays—most heavy quark experiments have silicon detectors for front-ends, and it is difficult to reduce the amount of material beyond a minimum of typically a few millimeters of silicon. However, a pretrigger based on electromagnetic p_T deposition, in conjunction with a higher-level prompt electron identification trigger, may be feasible.

F1.2 - Transverse energy deposition

This technique has been employed successfully in fixed-target experiments that studied charm production. It has the attractive feature of being the least biased, while still enhancing the signal-to-background ratio. However, it is too "loose," and results in an undesirably large data set with a large burden on the off-line analysis. It is expected that at the SSC, limitations on the rate of data acquisition would result in a high threshold for the deposited energy, thereby cutting out a large fraction of signal events. This method also necessitates the inclusion of a hadronic calorimeter in the detector design, which may not be absolutely essential for measuring the final state particles. Hence, at best, the inclusion of a crudely segmented and instrumented wall that acts as an absorbing shield for the muon detector can be recommended, in order to provide a fast pretrigger. The threshold can be set so that it provides a rejection level of the order of 10–100 over minimum bias interactions. As mentioned earlier, an electromagnetic p_T pretrigger may serve the same function for a large fraction of the events.

F1.3 - Strangeness trigger

Cascades of B decay will have a kaon in the final state in most of the cases. Any design of a spectrometer for studying B production is almost certain to include a particle identification detector, specifically for $K/\pi/e$ separation. It is quite likely that the detector will be a Cherenkov Ring Imaging Detector (CRID). Considerations of rate make it seem likely that a CRID will have to be operated so that it is gated by a first-level trigger. Hence, even though it may be possible to implement fast algorithms combining tracking and CRID information for triggering on kaons, it will have to enter as a second-level trigger, and in that case is probably not very useful. In any case, at the SSC energy scale, a kaon in the final state may not provide any suppression over minimum bias events.

F1.4 - J/ψ trigger

The possibility of triggering on J/ψ production via its decay into dilepton channels is an attractive option, because at the SSC energy scales a large fraction of the J/ψ production is via the decay of B mesons. Since the $J/\psi K^\circ$ channel is one of the CP eigenstates being considered, this is a natural choice for triggering. In addition, a measurement of $J/\psi K^+$ and$J/\psi K^-$ modes allows for measurement of the ratio of B^+/B^-production cross section. This in turn can be related to the ratio of inclusive

$\overline{B}^{\circ}/B^{\circ}$ production. Previous fixed-target experiments have successfully employed triggers with an adjustable dimuon mass threshold. This is relatively simple to implement, and does not suffer from large backgrounds. The dielectron channel may not be easily accessible, primarily because of the high background from the continuum of converted photons, and possibly because of a high combinatorial background of electromagnetic showers in the event. In order to alleviate the latter problem, rather elaborate instrumentation is required for a fast electron identification.

F1.5 - Multivertex event topology

This is the most direct—and also the most challenging—method for triggering on heavy quark production. At the SSC, this may be the only method for triggering on rare branching modes, such as $B^{\circ} \rightarrow \pi\pi$ and other two-body decays, which are also essential for studying CP violation. The background for two-body decays from $K^{\circ} \rightarrow \pi\pi$ and charm decays may be quite large, and requires further investigation. Of greater concern is the background rate of "fake" two-body vertices formed by projecting low-momentum tracks that have undergone multiple Coulomb scattering in the beam pipe and the silicon detectors. Employing silicon pixel detectors, as opposed to silicon strip detectors, should provide an advantage in reducing this background, because it is less likely that three-dimensional tracks will produce an apparent vertex. Inability to trigger on the rare decays directly implies that it is necessary to rely on triggering on the semileptonic decay of the partner B, and then suffer a large loss of statistics to find the rare modes in the data sample off line.

Various algorithms have been suggested for flagging an event containing a secondary vertex. The processing speed of these algorithms determines the trigger level at which they can enter. At a luminosity of 10^{32} cm^{-2} s^{-1}, there is, on the average, a time interval of 100 ns between two interactions. Most of the algorithms currently proposed require a processing time in excess of 10 μs. This limitation comes not only from the processing speeds of the available processors, but also from the rate at which data can be read out. From these simple considerations, it follows that these processing times require that the pretrigger provide a reduction of a factor of 10^{-2} to 10^{-3} over minimum bias interactions. It is foreseen that with the availability of faster components, considerable improvements in performance versus rate can be achieved. Due to the problem of multiple Coulomb scattering, it may be necessary to have a two-level vertex trigger, wherein the first-level flags events based only on apparent topology, and the second level incorporates momentum information and performs a fit for the vertex solutions.

F2 - Trigger Architecture

In the following, an architecture based on the preceding arguments is outlined. An attempt has been made to fully exploit the rate capabilities, so that the trigger is able to perform even at luminosities exceeding $10^{32}\,\mathrm{cm}^{-2}\,\mathrm{s}^{-1}$, which may be desirable for special purpose running. The trigger architecture has to be intimately connected to the data acquisition philosophy, so we assume that the key components of the spectrometer—the vertex detector and the muon system—are capable of pipelining their data in the event of a level-zero or a level-one pretrigger. The trigger architecture is discussed with only three levels conceived at this stage; however, any other architecture could be introduced in parallel without a major penalty in terms of live time.

F2.1 - Level Zero

There are two outstanding candidates for the level-zero trigger that can be run in parallel; namely, transverse energy deposition and single muon. The desirable rate for these pretriggers should provide a reduction over interaction at the level of 10^{-2}–10^{-3}, if possible, and the formation time for these pretriggers should be of the order of tens of nanoseconds. Because of unknown factors in the calorimeter design, only the muon trigger is discussed in this section.

The simplest approach for implementing the muon pretrigger is to have resistive plate chambers (or scintillator paddles) sandwiched behind the hadron calorimeter and inside the shields for the muon system. However, fine segmentation will be needed to form coincidences in order to reject low-momentum punchthrough muons that have a trajectory incompatible with the assumption that the muons point to the interaction point. We have studied rates for muons from π/K decay as a function of the decay distance from the interaction point to the calorimeter. Minimum bias events were generated using the Monte Carlo program HERWIG v5.3, and the pions and kaons in the events were allowed to decay. The muons were restricted to lie in a 10° cone. No cut on the lowest value of angle was imposed, because it was assumed that the dipole magnet will kick even the most forward muons into the detector acceptance. The distributions of muon momenta for three different decay lengths are shown in Fig. F.1. The desired suppression factor will dictate the amount of absorber material that is placed in front of the muon system, which in turn will define the efficiency for detecting muons from B decay. In Table F1, rates of muons-per-event are listed for the three values of cut on the momentum. It can be seen that for a 10 m long detector, the muon rate above 15 GeV/c is 7.6×10^{-2}, which translates into a muon flux of 760 KHz. A length of 10 m is quite reasonable for a detector that has to be both a good tracker and a good particle identifier. The amount of absorber material required for ranging out muons below 15 GeV/c is already quite high, and the consequences due to multiple Coulomb scattering may restrict the addition of any more absorber. Due to lack of detailed Monte Carlo programs, simulations of punchthrough muons

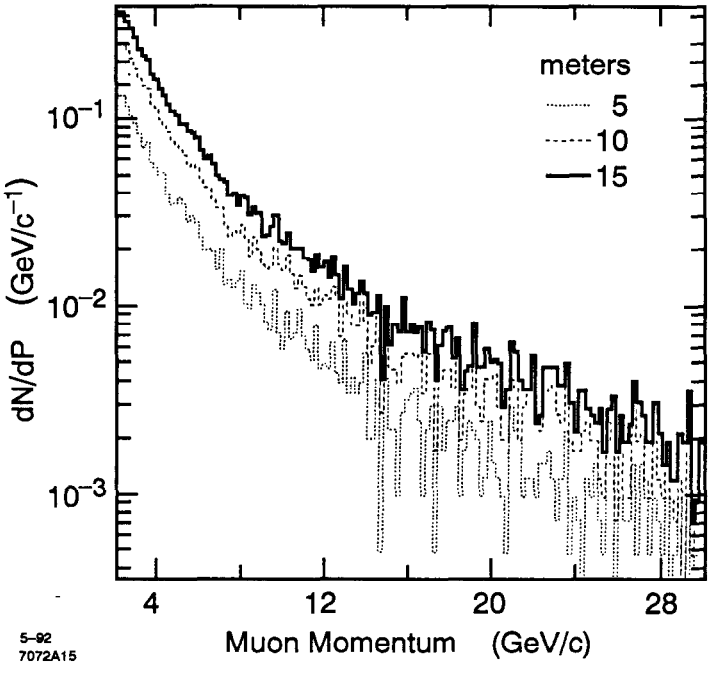

Figure F.1. The muon momentum distribution per event (per GeV/c) from decays of pions and kaons. Three different decay lengths are considered. The plot is normalized to the total number of minimum-bias events generated.

Table F1 - Rates of muons-per-event from decay of pions and kaons for various decay lengths and momentum cuts. Simulation errors are of the order of 2%.

	Muons per event			
Decay length	No P cut	$P > 5$ GeV/c	$P > 10$ GeV/c	$P > 15$ GeV/c
5 m	0.60	0.14	0.06	0.036
10 m	1.15	0.28	0.13	0.076
15 m	1.68	0.42	0.19	0.116

have not been performed. The spectrum of muons from B decay is shown in Fig. F.2a, and the loss due to various cuts is shown in Table F2. A 15 GeV/c cut can be read to impose an additional loss of 24% for muons in a 10° cone.

Clearly a rate of 760 KHz (nearly one pretrigger every microsecond) is too high for a vertex or J/ψ mass trigger, and an additional reduction in rate is required. Further suppression can be achieved by imposing a cut on the transverse momentum

Table F2 - Acceptance of muons from decay of B mesons with successive cuts applied.

Cut	Fraction surviving
10° cone	24.6%
$P > 5$ GeV/c	23.2%
$P > 10$ GeV/c	21.0%
$P > 15$ GeV/c	18.6%
$p_T > 1$ GeV/c	14.6%

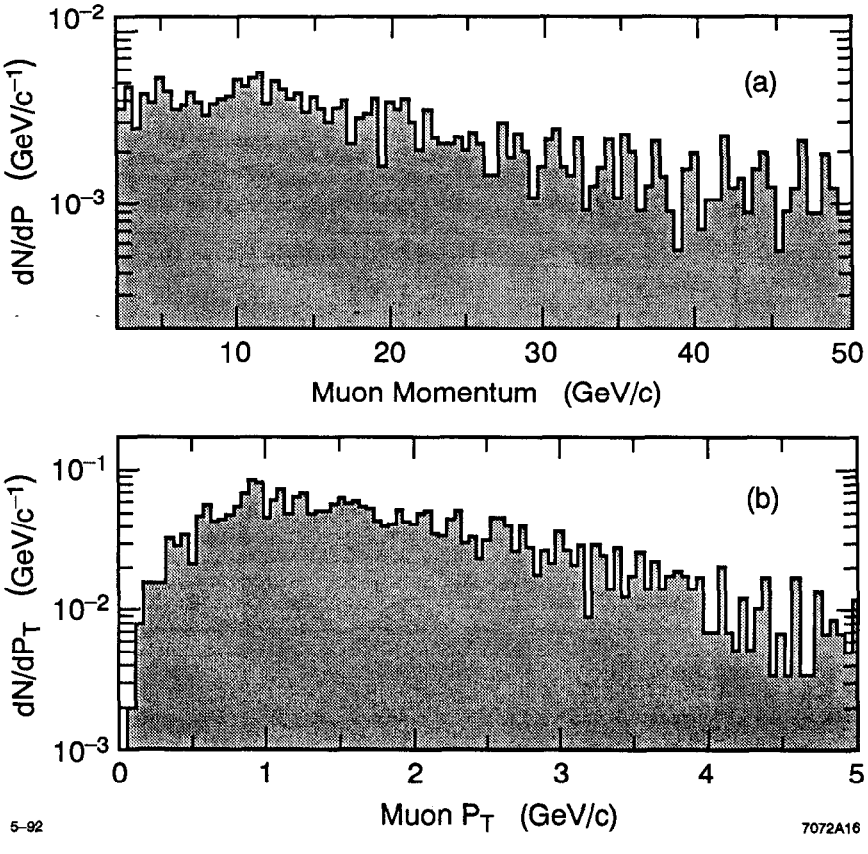

Figure F.2. (a) Distribution of muon momentum per GeV/c from the decays of B mesons, and (b) distribution of the muon transverse momentum (p_T) for muons with a momentum above 15 GeV/c from B meson decays, with both (a) and (b) normalized to the total number of $B \rightarrow \mu X$ events generated (X meaning anything)

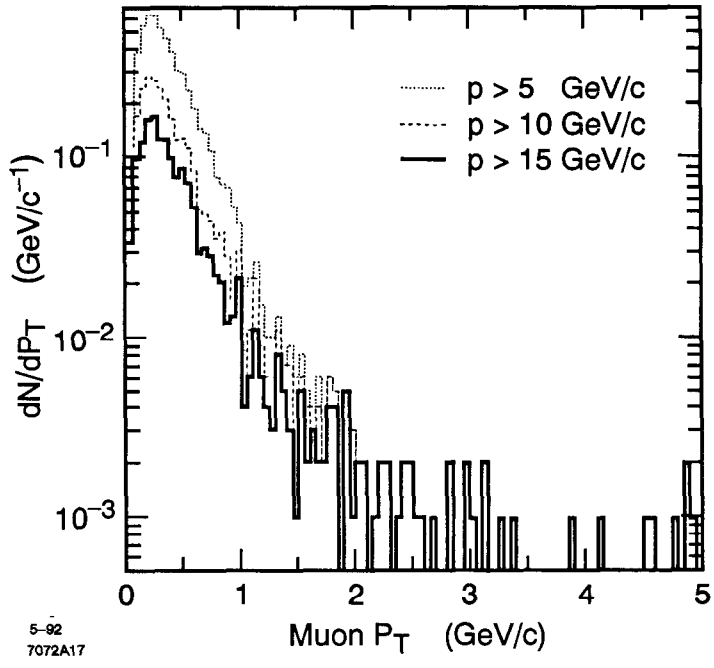

Figure F.3. Transverse momentum (p_T) distributions for muons above some momentum cuts and from the decays of pions and kaons. Three different values of the momentum (p) cut are considered. The plot is normalized to the total number of minimum bias events generated.

of the muon. This would require a fast calculation of the p_T, and a method for doing that is discussed in the next section. The p_T spectra for a 10 m long detector and various muon momentum cuts is shown in Fig. F.3. If a muon momentum cut of 15 GeV/c is chosen, then the rate above a p_T of 1 GeV/c is 6.2×10^{-3}. The resulting cut in the B decay spectrum is an additional 21%, as can be seen from Fig. F.2b and Table F2. In summary, this trigger choice is capable of providing a background suppression of 6.2×10^{-3} and an overall efficiency of approximately 15% for muons from B decay.

The formation time of the pretrigger may impose the ultimate limit on luminosity. The discriminators, coincidence logic, or summation circuitry will be placed close to the detectors, and should be able to form a signal in approximately 30 ns. Additional delay will come from fanning out this signal to the detector planes. This delay should not be any longer than 20 ns. This signal will then initiate the data digitization and readout for the muon system. For the purpose of the trigger algorithms, it is assumed that each channel of this system that is above some threshold sends out its unique address and contents to the trigger processors. The detectors that are not involved in the trigger are assumed to have the capability of time-stamping and storing their events in a buffer for a duration that is equal to the formation time of the level-one trigger.

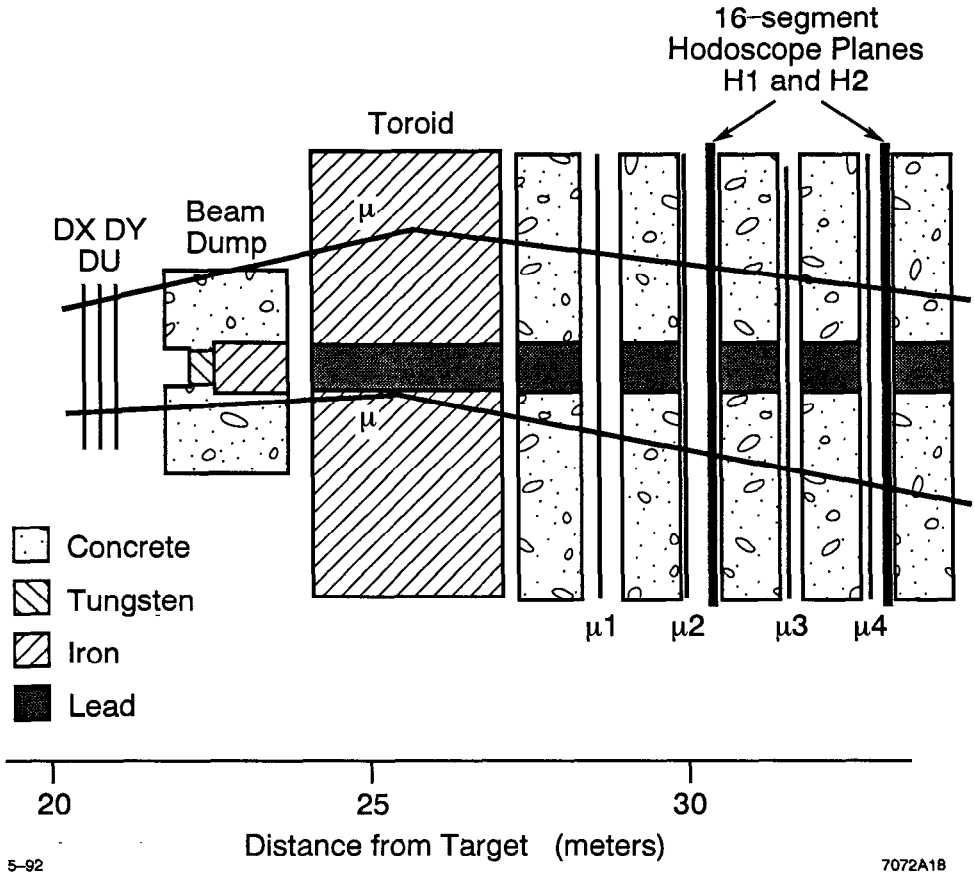

Figure F.4. The toroid-based E672 dimuon spectrometer. The hodoscopes and the muon detector planes are shown.

F2.2 - Levels One and Two

The most attractive candidates for the level-two trigger that can be run in parallel are the J/ψ trigger and the multivertex trigger. Various algorithms for the multivertex trigger are under study, so here we discuss only the J/ψ case. The trigger processor for the J/ψ can provide single muon p_T or multimuon triggers as by-products at level one. At a luminosity of 10^{32} cm^{-2} s^{-1}, the level-one pretrigger is expected to fire every 10–100 μs. The processing time goal for the level-one trigger should be well under a microsecond. Since the level-one and level-two triggers for this case are intimately related, they are discussed simultaneously in the following.

It is fairly straightforward to implement the J/ψ trigger in a few microseconds. It is interesting to note that a spectrometer for forward B physics at the SSC is very similar to a fixed-target experiment at the Tevatron. An interaction rate of 10 MHz is also quite typical. An example of a J/ψ trigger is employed by the E672/E706 experiment at Fermilab. Figure F.4 shows the essential components of

the toroid-based spectrometer located behind a large liquid-argon calorimeter. Only a muon with a momentum greater than 15 GeV/c could traverse the entire detector. A two-muon pretrigger provided by scintillator hodoscopes initiated the down-loading of all chamber hits into a CAMAC based processor, which computed momenta for the muons and a resultant invariant mass. The processor provided a 93% efficiency for triggering on J/ψ, with a mass resolution of 550 MeV/c^2. The processing time was 10 ms and, at an interaction rate of 1.5 MHz, this scheme provided an overall rejection factor of 2.5×10^{-5} for a mass threshold of 1.0 GeV/c^2.

Figure F.5 shows the outline for a similar architecture for the SSC that employs large look-up tables in the trigger processor. For convenience, it is assumed that each plane of the muon detector has its sensitive elements grouped into 256 strips in each view for the purpose of triggering. When a level-zero pretrigger fires, the strips above threshold in four planes send their unique 8-bit address to an encoder that forms 32-bit addresses from all combinations and enters them into a pipeline. Note that the address formation includes three-hit combinations as well. The actual number of combinations will depend on the noise levels and inefficiencies of the detector planes, but it is safe to assume that this number will typically not exceed ten for single muon events. The addresses are used to read a 16 GByte look-up memory, where nonphysical solutions are rejected and valid track parameters are put into the pipeline. With 30–50 ns access time for the memory, the worst case event should not take more than 300–500 ns for the look-up process, and considerably less for quieter events.

It is straightforward for the look-up memory to contain a value of p_T corresponding to its true value projected onto one view. Some error in this value is imparted due to magnetic fields upstream of the muon system, which can be partially corrected for, and some error is also due to multiple Coulomb scattering in the intervening material. Additional constraints can be obtained by requiring a p_T above threshold in two out of three views.

Note that due to the pipelined nature of the processor, only channels with valid information are busy (for the duration that it takes them to send their information), and all the other channels are active. In any case, this system should be able to handle a level-zero rate of 760 KHz, as estimated earlier.

Since this level-one trigger occurs every 160 μs or so, it should be safe to latch the rest of the experiment with this signal. For the case of the level-two vertex trigger, additional cost in time delay would come from the propagation of the signals to the vertex detector that is the most upstream element; it can be estimated to be no more than 80 ns. Hence, the vertex detector, and the rest of the spectrometer, should be capable of storing events for 1–2 μs at most.

The next stage in the pipeline is a mass processor that combines track information from the crossed views and correlates them with hit information from the stereo view(s). As exemplified earlier, this scheme can result in a mass resolution of a few hundred MeV/c^2, even with a segmentation of 256 elements per detector plane. The processor itself will add at most a few microseconds. The overall time should be well within 10 μs, which represents less than 10% dead time. Needless to say, detailed simulations of rates, resolutions, time delays, and thresholds are required.

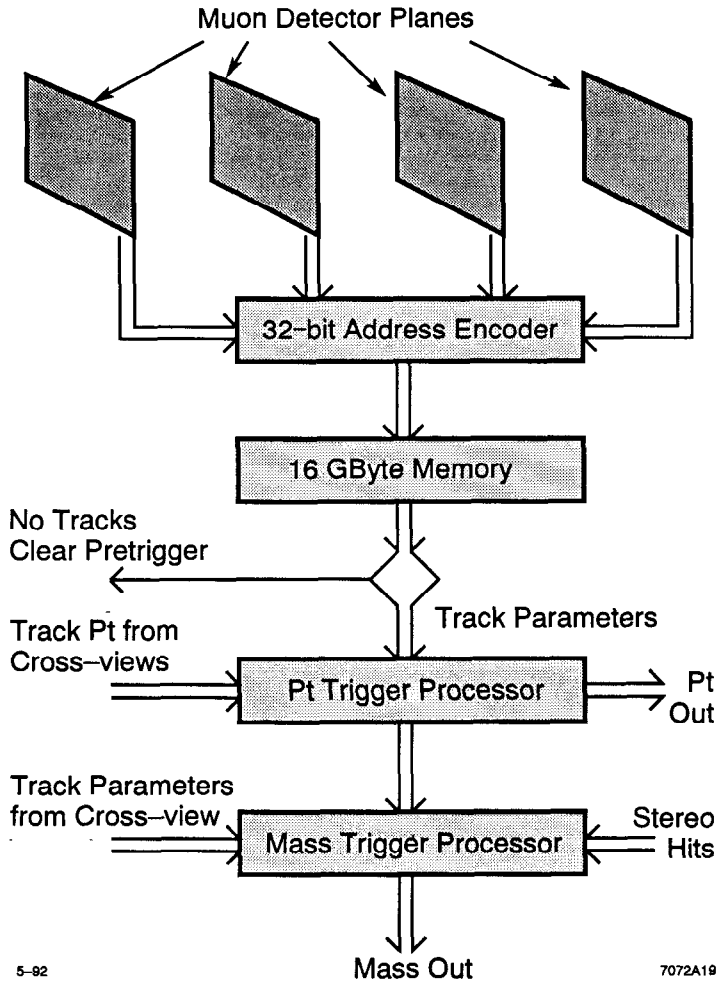

Figure F.5. Box diagram of a trigger architecture for a level-one p_T trigger and a level-two mass trigger. The level-zero pretrigger is not shown.

F3 - Conclusions

The most promising trigger for study of CP violation using a forward spectrometer at the SSC is a level-one muon p_T trigger that provides a background suppression of 6.2×10^{-3} and an overall efficiency of approximately 15% for muons from B decay. In addition, J/ψ and multivertex triggers are attractive because they will reduce the data set considerably. Both of these triggers require a level-one pretrigger that can provide 10^{-2} to 10^{-3} rejection over minimum bias events. The important variables for achieving this suppression are the muon momentum cutoff and the transverse energy threshold, both of which can potentially reduce the signal rates as well. Hence, a detailed study of pretrigger rates lies on the critical path toward a design for a spectrometer.

Appendix G

B Mass Resolution

G1 - Estimate of the errors

A study was undertaken of the B meson mass resolution for two- and four-body decays, using the detector described in Section 4.4. We considered decays where only charged particles are in the final state. Events were generated with a center-of-mass energy of 40 TeV using ISAJET with the B_d^0 being forced to decay via the following two modes:

$$B_d^0 \rightarrow \pi^+\pi^-$$

$$B_d^0 \rightarrow \bar{D}^0 K^{*0} \rightarrow 2K^+ 2\pi^- \quad .$$

Only events where all the decay products had a pseudorapidity between 2.4 and 4.7 ($1 < \Theta < 10°$) were accepted. In addition, all B decay tracks were required to have a momentum greater than 5 GeV/c. The decay particles were tracked through the silicon pixel detectors and the tracking system in the magnetic field. The error in the angle measurement of the tracks due to the pixel detectors is, in principle, due to the multiple scattering and spatial resolution. In practice, only the multiple scattering contributes to the error, since the spatial resolution at a pixel disk is ~ 5 μm.

The momentum resolution due the tracking detectors in the magnetic field, is given by the following expression[19] (the quoted references are those given in the text):

$$\left(\frac{\delta p}{p}\right)^2 = \frac{720}{n+5}\left(\frac{\delta x p}{3\times 10^{-4} B_K l^2}\right)^2 + 1.43\left(\frac{0.015}{3\times 10^{-4}\beta B_K l}\right)^2 \Sigma_{i=1}^{n} t_i \left(1+\frac{1}{9}\log\, t_i\right) ,$$

where p refers to the momentum of the track (in GeV/c) transvere to the magnetic field B_K (in KG), while l is the length of the track in the magnetic field (in cm). This formula is valid for $n > 10$ measurements per track where each of the detector elements has a thickness t_i in radiation lengths and a spatial resolution of δx (in cm). Note that $\beta \sim 1$ is the velocity of the measured particle. The first term in the equation above corresponds to the error of the spatial resolution of the tracking device, while the error due to multiple scattering introduced by the second term is nearly a constant for the measured tracks. The equation can then be written in the more familiar form

$$\left(\frac{\delta p}{p}\right)^2 = (Ap)^2 + C^2 ,$$

where the A and C parameters depend on the spectrometer.

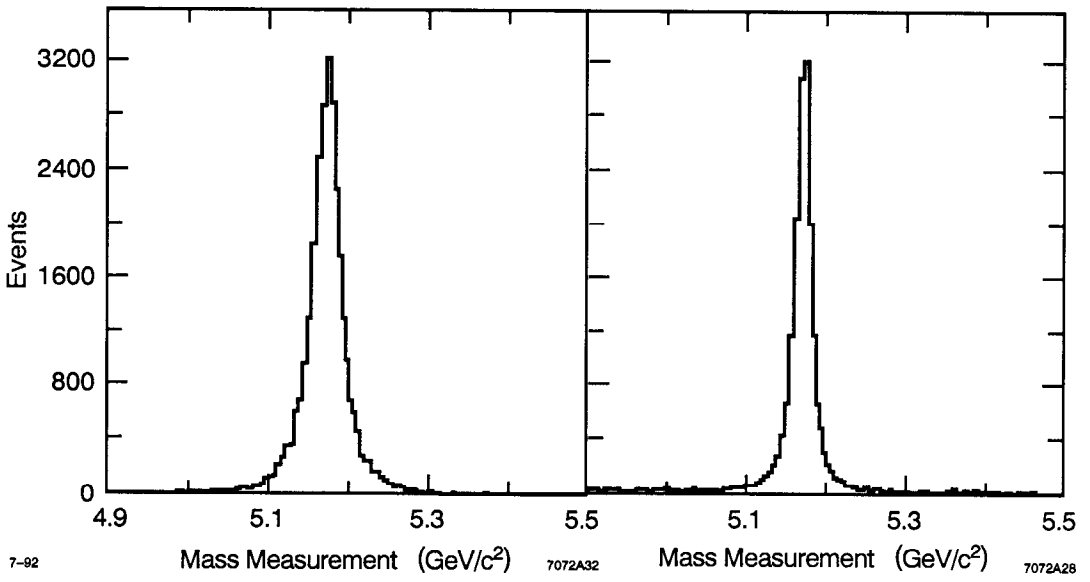

Figure G.1. Distribution of the B_d^0 mass measurement for (a) the $B_d^0 \to \pi^+\pi^-$ decay and (b) the $B_d^0 \to \bar{D}^0 K^{*0} \to 2K^+2\pi^-$ decay. The calculations were made with the spectrometer model discussed in Section 4.4.

In Fig. G.1, we show the calculated B mass distribution for the two channels under study, using the following parameters:

$$n = 50 \text{ planes}, \quad \delta x = 100\ \mu\text{m}, \quad l = 3\ \text{m}, \quad B_K = 20\ \text{KG},$$
$$\text{and} \quad t_i = 10^{-3} \text{ radiation length}.$$

With these values, we obtain $\delta M/M = 5.2 \times 10^{-3}$ ($\delta M = 27$ MeV) for the two-body decays and $\delta M/M = 4.5 \times 10^{-3}$ ($\delta M = 23$ MeV) for the four-body decays. Here, M represents the B meson mass. In Fig. G.2, $\delta M/M$ is shown as a function of the number of planes (n). One sees from this figure that the dependence of $\delta M/M$ is small for $n > 40$. We also present $\delta M/M$ (in Fig. G.3) as a function of the spatial resolution of the tracking system in the magnetic field.

G2 - Summary

We study the B_d^0 mass resolution for the decay modes $B_d^0 \to \pi^+\pi^-$ and $B_d^0 \to \bar{D}^0 K^{*0} \to 2K^+2\pi^-$. The study uses an example of a simple detector that was discussed in Section 4.4. With the present model, the mass error for the two cases is estimated to be small—$\delta M = 27$ and 23 Mev, respectively. These values may lead to a small background in the identification of the B_d^0 for these decay channels.

We also note that δM has little dependence on the number of planes (n) in the magnet for $n > 40$. In contrast, precision depends strongly on the spatial resolution of the tracking system in the magnetic field. Clearly, further detailed investigations have to be done in order to consider a realistic detector.

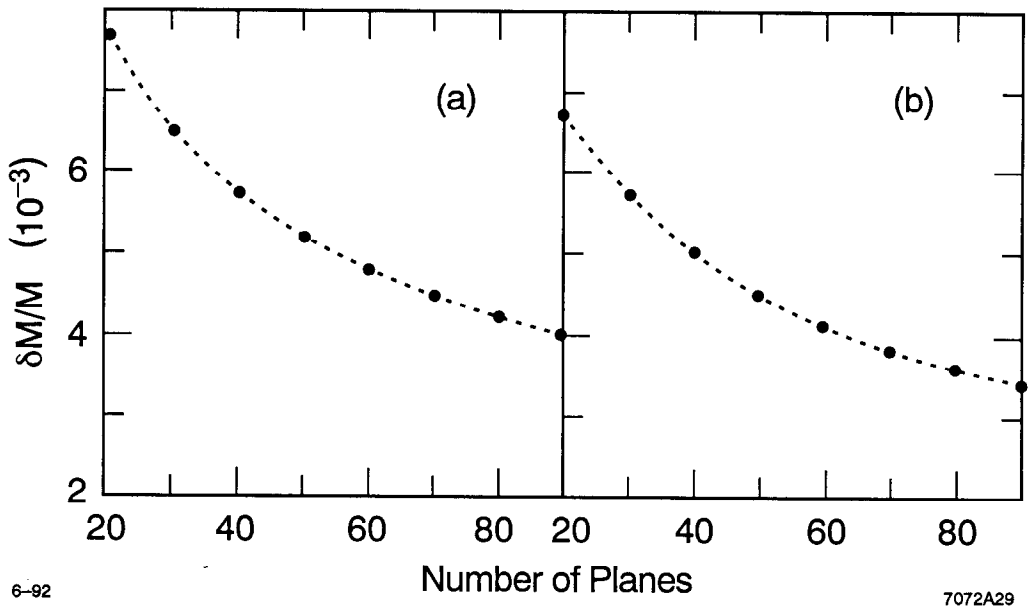

Figure G.2. Fraction of the mass error ($\delta M/M$) as a function of the number of planes in the magnetic field, for (a) $B_d^0 \to \pi^+\pi^-$ and (b) $B_d^0 \to 2K^+2\pi^-$.

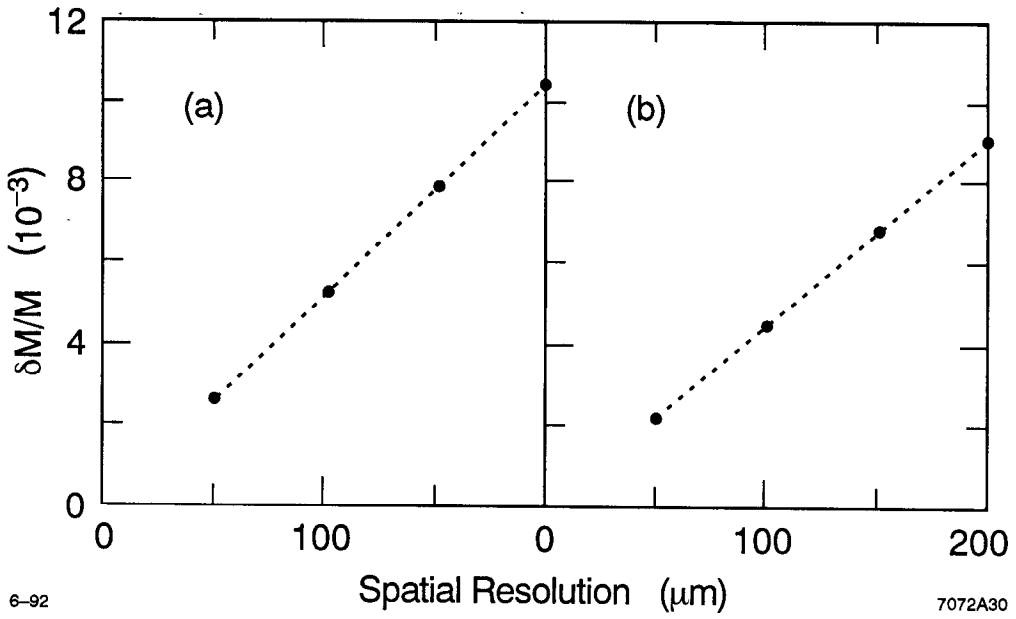

Figure G.3. Fraction of the mass error ($\delta M/M$) as a function of the spatial resolution of the tracking system in the magnetic field, for (a) $B_d^0 \to \pi^+\pi^-$ and (b) $B_d^0 \to 2K^+2\pi^-$.